Development and Evaluation of a Laboratory Water Pump Simulation with Measurement Uncertainty for Enhanced Learning

by

Ziming Zhong

A Thesis Presented in Partial Fulfillment
of the Requirements for the Degree
Master of Science

Approved July 2023 by the
Graduate Supervisory Committee:

Ryan J. Milcarek, Chair
Joshua D. Wilbur
Robert Wang

ARIZONA STATE UNIVERSITY

August 2023

ABSTRACT

Expedited by the ongoing effects of the Covid-19 pandemic and the expanding portfolio of Arizona State University's online degree programs, this study undertakes the task of enriching the “Experimental Mechanical Engineering” course within ASU's online Bachelor of Mechanical Engineering curriculum. This thesis outlines the development of simulations accurately mirroring the characteristics and functionalities of water pump laboratory experiments, which previously necessitated on-site, group-based participation. The goal is for these simulations to serve as digital twins of the original equipment, allowing students to examine fundamental mechanical principles like the Bernoulli equation and Affinity Laws in a virtual, yet realistic setting. Furthermore, the simulations are designed to accommodate uncertainty calculations, replicating the instrument error (i.e., bias and precision uncertainty) inherent in the original water pump units. The methodology of this simulation design predominantly involves the use of MATLAB SimScape, chosen for its configurability and simplicity, with modifications made to match the original experiment data. Then, subsequent analysis of results between the simulation and experiment is conducted to facilitate the validation process. After executing the full laboratory procedure using the simulations, they displayed rapid operation and produced results that remained within boundaries of experimental uncertainty, it also faces several challenges, such as the inability to simulate the pump cavitation effect and the lack of animation. Future research should focus on addressing these limitations, thereby enhancing the model’s precision and extending its functionality to provide better visualization capabilities and exploration of pump cavitation effects. Furthermore, students’ feedback

needs to be collected, since it is essential to assess and validate the effectiveness of this instructional approach.

TABLE OF CONTENTS

Page

CHAPTER Page

APPENDIX Page

LIST OF TABLES

LIST OF FIGURES

Figure Page

Figure Page

Figure Page

Figure Page

Figure Page

CHAPTER 1

INTRODUCTION

The evolving landscape of engineering education, accelerated by challenges such as the global COVID-19 pandemic, has demanded the need for adaptable and accessible teaching tools. This thesis dives into one such innovation: the design of a simulated laboratory unit for a centrifugal water pump experiment, which is a part of the in-person laboratory course for engineering students at Arizona State University.

The necessity and importance of this design originates from multiple factors. Among these, cost and accessibility considerations take center stage, especially in the context of expanding online degree programs at ASU [1]. This water pump physical lab experiment is not only time-consuming but also financially burdensome; the cost of the mechatronic laboratory device developed by Turbine Technology for this course alone stands at a considerable amount, running into tens of thousands of dollars. Compounding this fiscal pressure, the water pump instrument also requires constant maintenance, a task handled by a full-time laboratory manager, further straining the original budget. Moreover, such device can be complex to operate, requiring strict procedures followed and careful handling to gather results. Especially during periods of social distancing, communication among group members becomes challenging [23]. The on-site laboratory device also limits number of occupants during testing to ensure the best observable result for students, prolonging the time spent. And the device compromises individual hands-on experience, as students are typically grouped into teams to complete the experiment.

In response to these challenges, and to adapt the course format to more students, including those enrolled in out-of-state online degree programs, the development of a simulated laboratory unit has become necessary. Before diving into the unique aspects and features of this virtual centrifugal water pump experiment, it's essential to provide an overview of existing remote laboratory designs. The table below categorizes these designs based on their engineering subjects and features, underscoring the distinctiveness of this project. Given that the Centrifugal Water Pump Simulation at the heart of this thesis is closely tied to Thermal Fluid topics, this review focuses specifically on innovations within and outside of these fields.

1.1 Engineering Courses with Virtual Problem Solving

In engineering education, various disciplines have already utilized simulation for computational analysis in courses. For example, in most fluid mechanics courses, software such as ANSYS is frequently used to help students analyze fluid flows. In solid mechanics, software is also used to analyze stress distributions given material properties, loads, as well as other inputs. Software like MATLAB Simulink & SimScape is capable of providing both numerical analysis and illustrations on individual parts or the entire system. Table 1.1 serves as a comprehensive overview of the integration of simulation software into various disciplines of engineering education. This table provides an array of engineering course topics, highlighting which tools like ANSYS and MATLAB are utilized. They effectively enhance the understanding of engineering education outcome.

Table 1.1 Engineering courses using simulation software

Thermal Fluid Topics	*Software*	*Derivation Method*	*Error Propagation*	*Interface Format*
Heat Exchanger, Tank Level Control & Mixing Tank & Temperature Control [2]	MATLAB GUI	Governing Equation	N/A	2D Schematics
Uncertainty in Heat Exchanger & Tank Volume [3]	MATLAB GUI	Governing Equation	N/A	2D Schematics
DLMX Heat Exchanger [4]	MATLAB Simulink, LabVIEW	Governing Equation	N/A	2D Schematics
Transient Heat Transfer [7]	MATLAB GUI	Governing Equation	N/A	Graphical Analysis
Crossflow Heat Exchanger [6]	MATLAB Simulink	Governing Equation	N/A	2D Schematics
PEM Fuel Cell [5]	MATLAB Simulink	Governing Equation	N/A	2D Schematics
Other Engineering Topics	*Software*	*Derivation Method*	*Error Propagation*	*Interface Format*
Aircraft Rolling, Antenna Tracking [3]	MATLAB GUI	Governing Equation	N/A	2D Schematics
Dynamics	MATLAB Simulink	Governing Equation	N/A	2D Animation
Data Communication [8]	Java	N/A	N/A	Data Analysis
No Load Test on a Transformer [10]	PSoC LabVIEW	N/A	N/A	2D Animations

By analyzing Table 1.1, we can deduce that the incorporation of simulation software in engineering education not only has become a standard practice across disciplines, but it also fosters interactive learning. The tools allow students to visualize concepts, apply theories in practical scenarios, and scrutinize system interactions - all of which cater to diverse learning styles. Essentially, these examples in Table 1.1 have been categorized into thermal fluid topics and other engineering topics, and the detail of implementation for both categories is discussed below. However, the table also highlights the fact that measurement error and error propagation have not been considered in these previous simulations, which will also be discussed in greater detail below.

1.1.1 Thermal Fluid Topics

A study that summarizes four virtual experiments related to mechanical engineering topics - mixing tank, heat Exchanger, tank level control, room temperature control - emphasizes the simplicity and accessibility of the design by showcasing the schematics of the system and related governing equations. According to the feedback provided by the author, the use of a schematic interface coupled with input icons can save time for students without previous coding experience [2]. The same author later on did another study of four additional virtual laboratory examples, especially the topic of counteracting uncertainty in heat exchanger and tank volume demonstrates the importance of simplifying the simulated control system [3]. There are also other examples using simulation software as well as schematic interface. The University of Texas at Tyler had experimented with a simulated thermal fluid laboratory course [4]. The device they simulated is an Armfield DLMX Heat Exchanger that is capable of providing experiments on fluid mechanics, thermodynamics,

and heat transfer, but it lacks some properties measurements and data presentations. Thus, the simulation makes up for the missing measurements, and it generates data using LabVIEW. Then, the gathered data are transmitted to another interface using MATLAB Simulink based on governing equations for data analysis. In conclusion, the virtual experiment allows them to improve the accuracy of data, and it also provides more interactive results to students. The same team also conducted a second virtual laboratory design for the proton exchange membrane fuel cell in the same course development [5]. Their methodology this time is to design the entire model from scratch on MATLAB Simulink, so students may interact with the interface and simulated modules to enrich their knowledge in fuel cell as well as control theory. Judging from the result based on governing equations and PID controller using MATLAB Simulink, the design outputs anticipated data that are within the theoretical ranges. Lastly, the same team put together another virtual crossflow heat exchanger from scratch using MATLAB Simulink [6]. By applying the governing equations and assumptions of fluid flow, the output results are within 15% accuracy, and the schematic interface looks promising. The research group from Universidad del Atlántico has developed the virtual lab software using MATLAB [7]. Perhaps due to the nature of heat transfer courses, the graphical interface of their simulation only provides surface plots of transient heat transfer scenarios, requiring students to be adequately prepared for the principal knowledge beforehand. Still, they analyzed the outcome from doing statistical surveys on the feedback of participants, and most of the comments are positive. These analyses of various thermal fluid experiments demonstrate a wide spectrum of applied simulation tools, especially the MATLAB usage, underlining their efficacy in representing interactive thermal fluid dynamics and improving student

engagement. However, these examples do not consider the implementation of instrument uncertainty, a significant factor that students should encounter in physical laboratory.

1.1.2 Other Topics

The literature of simulation laboratory experiments in engineering education was also investigated in other disciplines, and most of the studies are for courses in electrical and control engineering with software simulations. The same team mentioned in section 1.2.1 that created simulations on various subjects in thermal fluids also conducted simulation experiments on aircraft rolling and antenna tracking [3]. The discussion provided by the author shows that such designs should help students to gain outstanding outcomes. The department in Covenant University, Nigeria came up with a Java-based virtual laboratory for data communication simulation [8]. Their aim for the project was to help students get more hands-on experiences in coding, modulation, and filtering, and to achieve it in a more affordable way considering the financial constraints they encountered. The instructor team from Rice University has implemented 2D animations to their simulated virtual laboratory course, which focuses on dynamical systems [9]. In addition, they ask students to participate in the modeling process after sufficient practices of MATLAB Simulink, Animation Toolbox, and schematics of the system, helping them familiarize analytical equations as well as dynamic control theories. Though there is not yet feedback from students, the well-planned teaching structure is said to be effective. Another study that investigates the result of simulating no-load test on a Transformer, which is an electrical engineering course experiment designed for students in India [10]. The outcome of conducting such research looks promising, because with the interconnection between the

simulation software as well as the physical chips, they were able to generate acceptable results. In addition, the 2D animations can help students in terms of understanding and interactions of the physics behind it.

1.1.3 Application of Virtual Laboratory

Besides software-based simulation methods, some universities and organizations also attempted using other formats of virtual laboratory. For example, educational institutions in India experimented with hybrid learning for mechanical engineering students [11]. They first trained the faculty members by giving instructions as well as practices of both simulated and remote triggered laboratories, then the students would run them and compare the results with real experiments conducted later on. By analyzing the differences in result between virtual laboratory and in-person laboratory, students gained better understanding of the physical model along with more interactive experiences. The faculties from Engineering Institute of Technology Perth, Australia also demonstrated a remote laboratory system (RLS), that is capable of remotely accessing all kinds of laboratory software and hardware for students [12]. While using the system, students can ask for help through the support ticket system and they have access to the related documentation. However, since the platform is fully virtual, students may find latency in compiling simulations, and the department may expect heavy funding for the maintenance. Still, the benefits of having such a system for online students are phenomenal, because the data analysis of both the results from experiments and the feedback from students compared to those in the original laboratories has ensured its feasibility and development. To be more

specific, students in low grade range tend to perform better with the help of RLS, and their experimental data matches closely to the ones conducted from the physical instrument.

1.2 Objective:

The aim of this project is to develop a simulation software interface for the laboratory water pump unit, thereby providing students the flexibility to interact with the system anytime, anywhere. The current laboratory water pump unit, manufactured by Turbine Technology and showcased in Figure 1.1, serves as the basis for this initiative. Drawing from the existing thermal fluids literature, and to facilitate an intuitive understanding of water pump mechanics and precise results, MATLAB SimScape is chosen as the modeling platform. Its built-in modules are rigorously documented by the MathWorks team, facilitating ease of use. The package also incorporates user interface implementation, further enhancing its user-friendliness. Unlike most thermal fluids literature, this project innovates by simulating potential instrument errors that could arise during real experiments due to human errors or sensor reading fluctuations. This injects an element of real-world unpredictability into the simulations, thus offering a more authentic learning experience. Taking cues from other engineering and virtual laboratory projects, this project also aims to enrich the educational experience through dynamic illustrations and online pedagogical resources. These include animations in video format and a dedicated course website for water pump experiment training, fostering a more interactive and engaging learning environment.

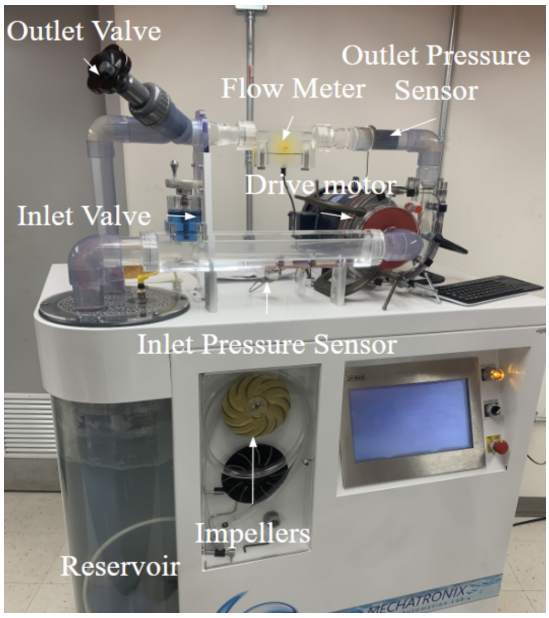

Figure 1.1. Physical laboratory unit developed by Turbine Technologies LTD [14]

1.2.1 Description of Water Pump Lab and Overlook of Digital Twin

Before starting with simulation modeling, the physical device must be analyzed. The original laboratory mechatronic device consists of multiple control units, including two primary tanks, reheater, different impellers, etc., but not all of them are applied to the mechanical engineering laboratory course. Thus, the virtual water pump design only focuses on the main components: centrifugal pump, impeller type, pipes, inlet and outlet gate valves, flow meter, torque sensor, and pressure sensor. As shown in figure 1.1, the drive motor is essentially the power source for the entire system. It converts electrical power to shaft power delivered to the pump, so the pump can convert that power into the mechanical power of the water through the impeller, and extract the water from the reservoir. The water flow starts from the reservoir, going through the inlet valve, experiencing suction and discharge from the centrifugal pump, passing through the outlet

valve, finally falling back to the reservoir. In the flow process, those mentioned sensors can record the data in the control panel. Now, to introduce the simulation project, the finalized design is showcased in figure 1.2, with a more detailed configuration and procedure of creation discussed in the next chapter. From figure 1.2, the simulation circuitry resembles the schematics of the water pump system: a velocity source that powers up the pump, with a torque sensor showing its torque readings, marking this part of circuitry dedicated to mechanical power conversion. The water is drawn from the reservoir by the pump, then the water flows back to the reservoir after going through inlet & outlet valve as well as the piping system. Corresponding flowrate sensor and pressure sensor output dynamic readings during the flow, representing this part of the circuitry as thermal fluid interaction.

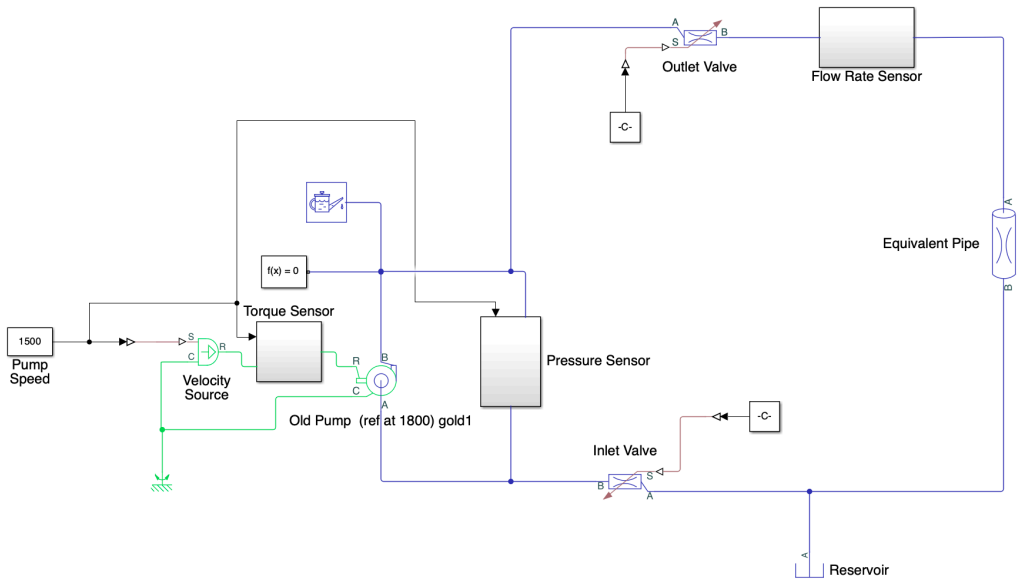

Figure 1.2. Simulation circuitry resembling gold pump (same circuitry for red pump)

Speaking of mimicking the real system, this simulated systems aims to generate equivalent data or a digital twin of the actual water pump lab unit. The digital twin concept was first mentioned by Dr. Michael Grieves in 2003. In his recent studies, he facilities the concept of digital twin, aside from the digital copy of the physical model, to be not only receiving real time data from the physical model, but it also can transmit data back to the physical model whenever the critical conditions such as indication of the maintenance are detected [13]. As shown in figure 1.3, since the accessibility of the original water pump equipment is ASU property, direct real-time data transmission can be challenging due to limited access between this instrument and external computers. Especially the backward data transmission (for data to be transmitted from the simulation back to the original water pump) is challenging for those reasons. Possible solutions are discussed further in the following chapters.

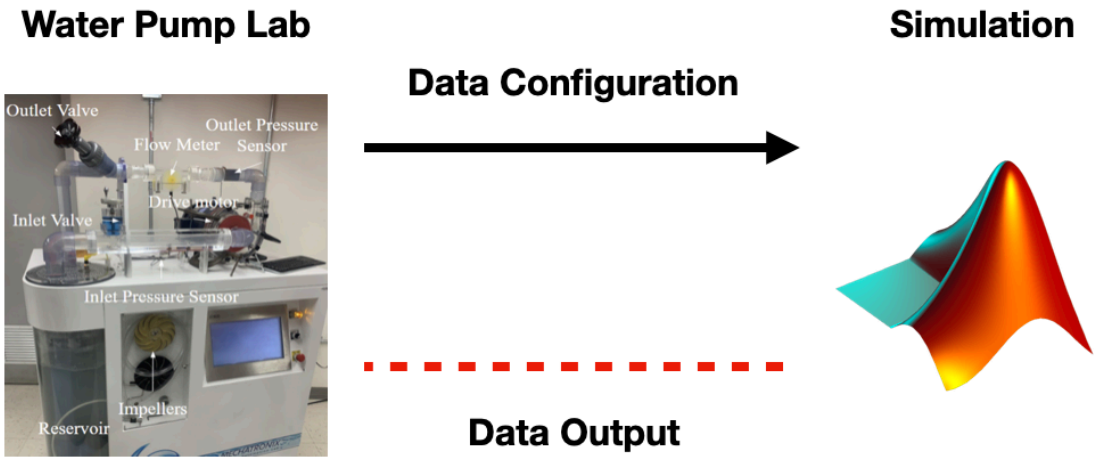

Figure 1.3. Digital twin criteria

1.2.2 MATLAB SimScape – Flexibility, Time and Cost Saver

Unlike all previous literature that includes MATLAB Simulink simulations, this project experimented on a more advanced package - MATLAB SimScape. It allows users to browse for the desired module and directly customize built-in modules to approximate the physical operating condition, dimension, etc. Not only does it save time for users in terms of defining governing equations, utilizing control theories, and mapping the circuitry, but it also has been verified and tested by MathWorks. Therefore, this project also assumes that the physics built in to the modules in the SimScape package have been verified. There are several major components that need to be simulated, all of which have pre-defined governing equations that can be found on MathWorks website. So once results are generated, they can be verified and validated quickly by testing the mathematics according to the website. On top of that, using such built-in modules has a great flexibility in customizing the desired scenario(s). For example, in the centrifugal water pump parameterization, users have three options to either type in analytical values for capacity, brake power, and total head or to type in 1D or 2D tabulated data that can be gathered from experiments, allowing the software to generate similar results compared to the actual data. The methodology of choosing the appropriate data parametrization is discussed in chapter 2, as well as the reason of implementing a modification to the pump governing equations.

1.2.3 User Interface & Schematics

The control panel in figure 1.4 illustrates the interface that students are interacting with during the physical experiment. To replicate that interface, as shown in figure 1.5, this

simulation improves the user interface with clear schematics closely resembling the actual laboratory unit, controllable knobs for the gate valve to adjust the flow rate, and unlike all previously mentioned literatures, this design also introduces instrument errors to the outputs by adding random noise factors. Upon proceeding to the simulation, students will be given video lectures assigned by the instructor that illustrate concepts as well as procedures from the lab manual [17]. During the virtual experiment, students can simply follow the lab manual to gather data step by step, preparing for further data analysis.

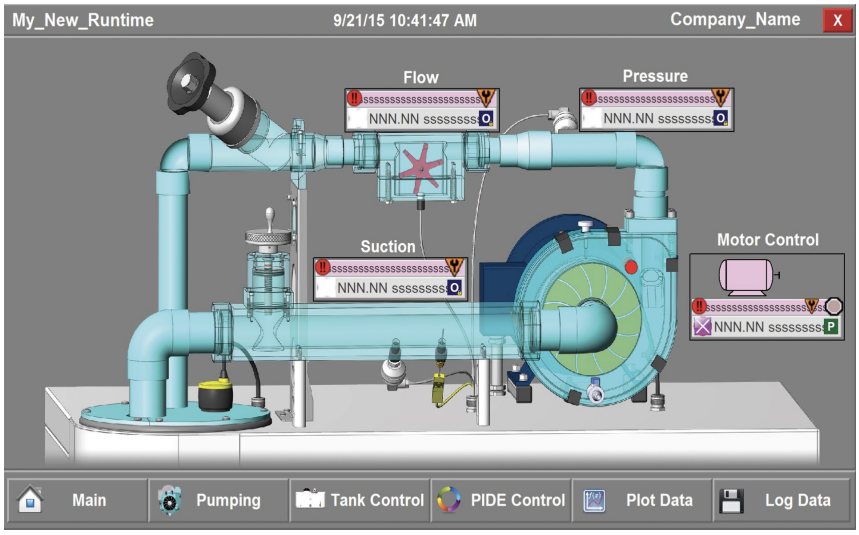

Figure 1.4. Original mechatronic device built-in interface [15]

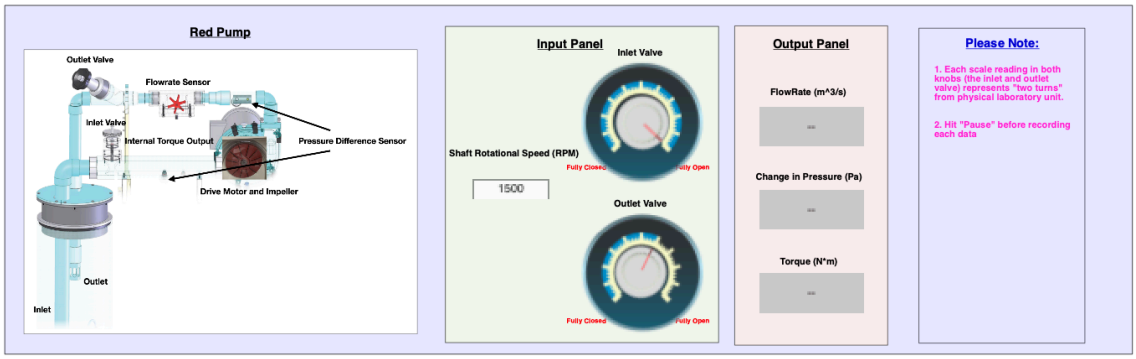

Figure 1.5. Example of simulation interface

1.2.4 Uncertainty:

Since the focus of the original mechanical engineering laboratory course is to explore the error occurring in measurements and other possible causes, bias and precision errors are introduced in the simulation. Also, based on the literature review presented in table 1.1, there has not yet been a single virtual experiment that addresses this topic, making this project design more original. The explanations of bias and precision errors are provided below.

Bias (B) refers to the systematic error that affects the accuracy of a measurement. It represents the difference between the true, as represented by the bullseye in figure 1.6, and the measured value, due to inaccuracy. Bias error can result from factors such as faulty instruments, calibration errors, or environmental conditions, and it is often quantified for a given system and provided in the manufactures specification sheet of a real system. In the experiment, the bias uncertainty of each data reading is a given by the lab manual.

Precision (P), on the other hand, refers to the degree of reproducibility or consistency in a set of measurements. It describes how closely repeated measurements of the same quantity cluster around the mean value and is usually evaluated as a standard deviation or standard error of the dataset. For example, a measurement with high precision produces results that are tightly clustered together, while a measurement with low precision produces results that are more widely scattered. In the experiment, the precision uncertainty is calculated using statistical analysis.

The total uncertainty takes account for both bias and precision uncertainty. It gives a range of values with a confidence level for the true value a system takes. For example, a measurement with high bias and low precision is said to be inaccurate, while a measurement with low bias and high precision is said to be precise and accurate. Students will explore their range once they complete analyzing their results.

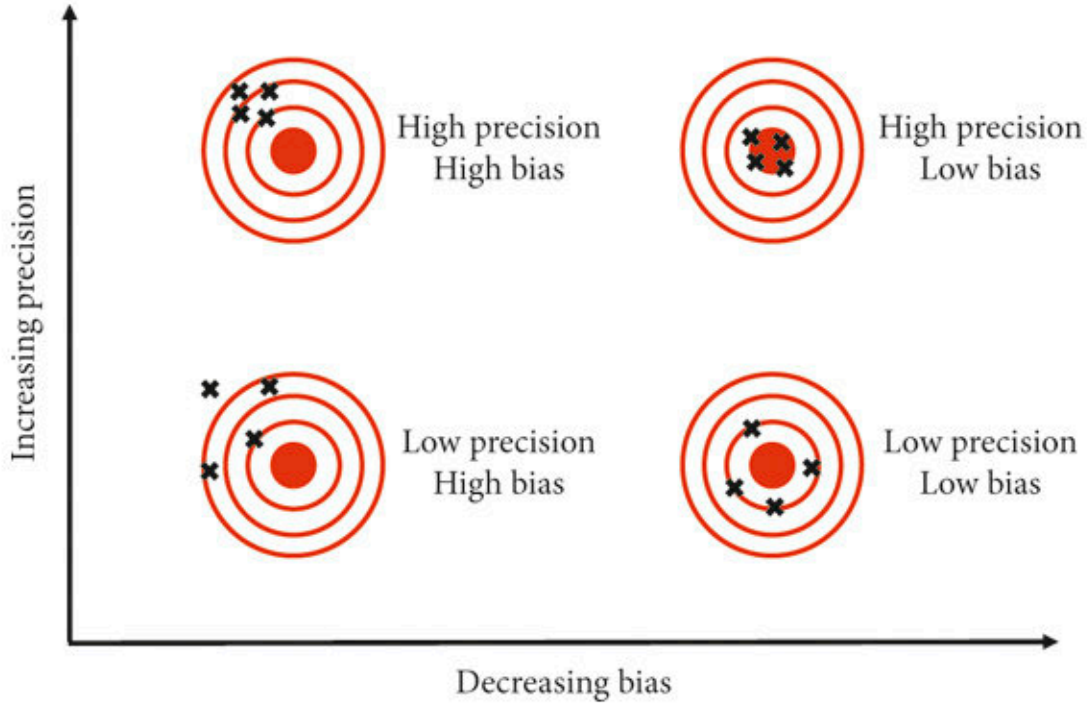

Figure 1.6. Terminology used in measurement [16]

CHAPTER 2

METHODOLOGY

From figure 2.1, a flow chart documenting the procedure for this thesis as well as students' curriculum is showcased. The developer's curriculum starts with writing the lab manual, which includes all necessary concepts and laboratory procedures. After completing the lab manual, it is necessary to conduct the entire physical experiment following the procedure in the lab manual. This step is critical because some of the data are used for simulation parameterization. After gathering necessary results from the physical laboratory, simulation is created based on detailed parameterization. Next, the simulation is tested with different setups to ensure the verification process, followed by necessary modifications. Finally, after the simulation is fully prepared for the experiment, the physical experiment procedure is applied on this simulation for result analysis. A cross validation between the actual experiment results and simulation results is made to ensure the accuracy. The students' lab procedure is not the focus of this thesis, but it is documented for clarity.

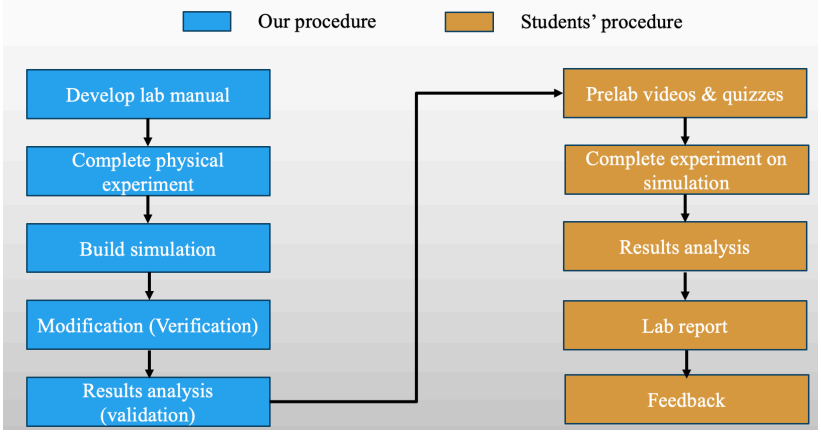

Figure 2.1. Methodology flow chart

2.1 Lab Manual:

The lab manual [17] has been developed in order for students to follow operating procedures. The parameters recorded are the pressure head, shaft horsepower (input), water horsepower (output), and efficiency of two centrifugal pumps. The total pressure head (H) is the result of static head, dynamic head, as well as friction head. The static head is the pressure required to pump the fluid against the gravity to the designated elevation. The dynamic head is related to the kinetic energy of the fluid, a result of fluid's flow. As for the friction head, it takes account for the piping geometry, viscous effect of the fluid, as well as other factors that impede the flow. The water horsepower (WHP) is a measure of power supplied to the water flow. The shaft horsepower (SHP) is the total electrical power delivered to the pump itself. As for efficiency of the pump, it is the ratio of WHP and SHP. The original laboratory contains two water pump units, as shown in figure 2.2, and the difference between them is the sweep vanes where the new one has red straight vanes and the old one has golden rearward straight vanes.

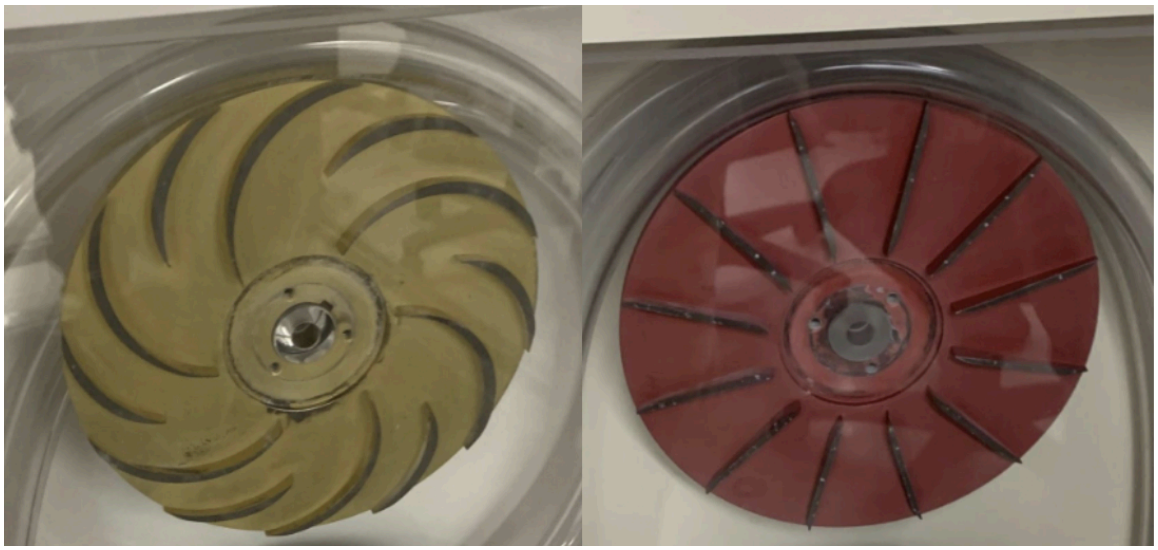

Figure 2.2. Gold impeller (left) and red impeller (right) [14]

In the original laboratory experiment manual part 1, students will investigate the pressure head, shaft horsepower, water horsepower, and efficiency of two centrifugal pumps equipped with a gold and a red impeller at the speed of 1200, 1500, and 1800 rotations per minute (RPM). To determine pressure head, WHP, SHP, and efficiency, they need to record the water flowrate, pressure difference between pumps' inlet and outlet, as well as the torque values at a constantly closing gate valve for both pumps. In short, by investigating the difference between the flowrate conditions, they can determine pumps characteristics as well as the effects of having different impeller vanes. In part 2 of the experiment, they will also investigate the iso-efficiency curve for both pumps by decreasing the pump speed without closing the gate valve from 1800 RPM all the way down to 300 RPM while recording water flowrate, pressure difference, and torque values, exploring the effect of pumps, flow condition, as well as impellers. Part 3 of the experiment is to explore the cavitation effect, which describes formation of bubbles existing in pipe segments where pressure is low. In this case, after closing the inlet at a shaft speed of 1650 RPM, the cavitation effect can be spotted near the pump inlet passage, potentially damaging the impeller. However, due to complexity as well as modeling constraint, this part of the experiment is excluded from the simulation for now.

In the simulation, students will still have the same objectives and need to follow the same procedure as in original laboratory procedure. Thus, there will be two simulations models for the experiment: one for the gold impeller and one for the red impeller. To structure the differences in impeller vanes, and to accurately represent both physical models, MATLAB SimScape built-in modules are desirable due to its configurability. As stated previously,

this simulation assumes built-in modules created by MathWorks are trustworthy, since all the centrifugal pump, pipes, as well as gate valve models are verified and documented by MathWorks themselves. One thing to notice is that this project uses isothermal liquid network (IL) modules, because the temperature is assumed to be fairly constant in the original experiment.

2.2 SimScape Module & Governing Equations:

This section details the derivation and parameterization, also known as "verification", of the main SimScape components used in the simulation.

2.2.1 Pipe (IL)

Pipe (IL) is a customizable component from SimScape package. This component assumes that the pipe wall is rigid, the liquid flow is fully developed, and the effect of gravity is negligible. From figure 2.3, the liquid will flow from port A to port B, and the parameterization is also shown. The reason to turn off the fluid inertia effect is that in pump parameterization, these effects can be calculated by the difference of one trial of experiment result vs. one trial of simulated result (curve fitting), propagating that difference into the remaining simulation so that the rest of the results can be adjusted accordingly. Such curve fitting method will be discussed further in the following sections. The dimensions come from the measurement of the real system, but it did not apply on the pipe length. The pipe length uses an "equivalent length" that represents the entire original

physical piping system as in figure 1.1. The elbow pipes and gate valve equivalent lengths are estimated according to the documentation [15]. Combining them and straight pipes can result in an approximately 2.5 meters long pipe. The simulation pipe can be found in Figure 1.2.

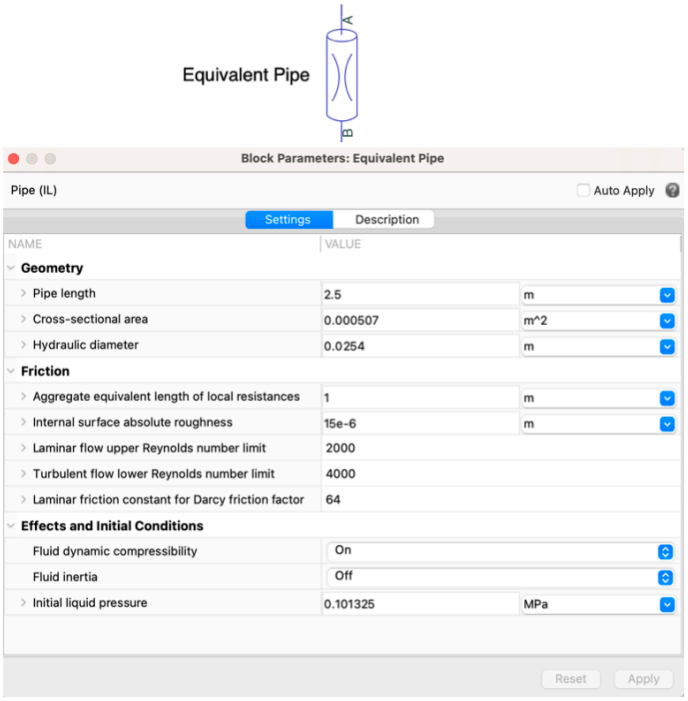

Figure 2.3. Equivalent pipe

The first governing equation for the Pipe (IL) according to the documentation from MathWorks [18] is the mass balance equation:

$$\dot{m}_A - \dot{m}_B = 0 \tag{2.1}$$

Where $\dot{m}_A$ is the mass flow rate at port A and $\dot{m}_B$ is the mass flow rate at port B.

The second governing equation for the Pipe (IL) is the momentum balance equation, note that the pipe is divided in half for each case:

$$p_A - p_I = \Delta p_{v,A} \tag{2.2}$$

$$p_B - p_I = \Delta p_{v,B} \tag{2.3}$$

Where p_I, p_A, p_B are the liquid pressures at intermediate point, port A, and port B respectively. $\Delta p_{v,A}$ and $\Delta p_{v,B}$ are the viscous friction pressure loss between the pipe volume center and ports A and B.

Meanwhile, the viscous pressure loss is represented as:

$$\Delta p_{v,A} = \begin{cases} \lambda\mu(\frac{L + L_{eq}}{2})\frac{\dot{m}_A}{2\rho_I {D_h}^2 S}, & if\ Re_A < Re_{lam} \\ f_A(\frac{L + L_{eq}}{2})\frac{\dot{m}_A|\dot{m}_A|}{2\rho_I D_h S^2}, & if\ Re_A > Re_{tur} \end{cases} \tag{2.4}$$

$$\Delta p_{v,B} = \begin{cases} \lambda\mu(\frac{L + L_{eq}}{2})\frac{\dot{m}_B}{2\rho_I {D_h}^2 S}, & if\ Re_B < Re_{lam} \\ f_B(\frac{L + L_{eq}}{2})\frac{\dot{m}_B|\dot{m}_B|}{2\rho_I D_h S^2}, & if\ Re_B > Re_{tur} \end{cases} \tag{2.5}$$

Where λ is the pipe shape factor which is used to calculate the Darcy friction factor in the laminar regime. μ is the dynamic viscosity of the liquid flowing through the pipe. L_{eq} is the aggregate equivalent length, representing the combined effect of local pipe resistances. D_h is the hydraulic diameter of the pipe. Re_A is the Darcy friction factor in the pipe halves adjacent to ports A. Re_B is the Darcy friction factor in the pipe halves adjacent to ports B. Re_{lam} is the Reynolds number at which the flow transitions from laminar to turbulent. Re_{tur} is the Reynolds number at which the flow transitions from turbulence to laminar.

2.2.2 Orifice (IL)

Orifice (IL) is another key component in the simulated piping system that mimics the gate valve controlling the inlet and outlet of centrifugal pump in the real experiment. It calculates how much the mass flow rate should become after going through the gate based on the defined opening position. In this case, the opening position is directly connected to the knob in the user interface as shown in figure 1.2. The figure 2.4 is the parameterization for both inlet and outlet gate valve.

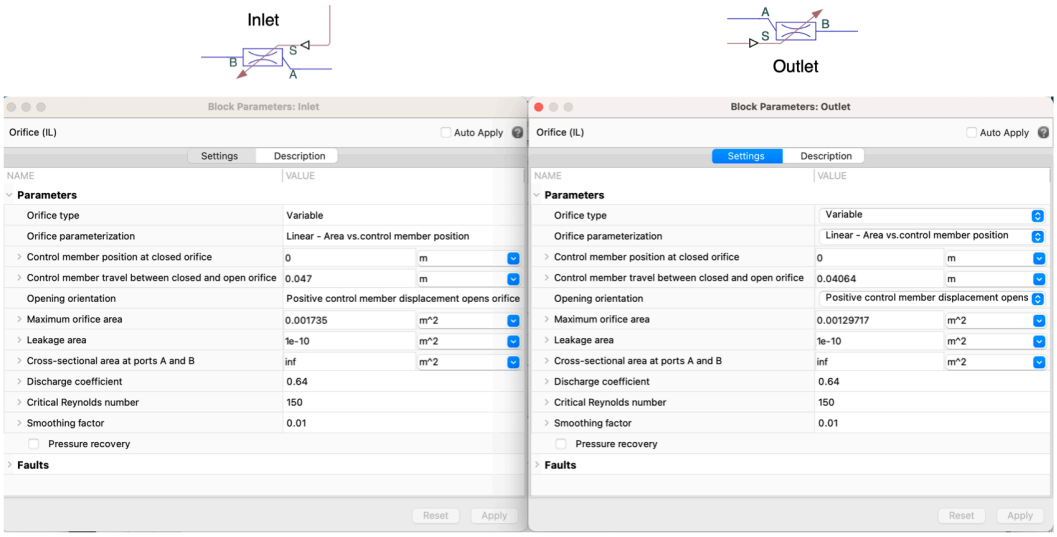

Figure 2.4. Gate valve configuration

According to the MathWorks documentation [19], the only governing equation for this block is the same mass balance equation as in equation 2.1. Since the opening area is variable based on the control member position, the open area is defined as:

$$A_{orifice} = \frac{A_{max} - A_{leak}}{\Delta S}(S - S_{min})\varepsilon + A_{leak} \tag{2.6}$$

Where S_{min} is the length of opening position when the valve is fully closed, ΔS is the length of control member travel standing position when the valve is being adjusted by the user, A_{max} is the maximum opening area, A_{leak} is the leakage area, ε is the opening orientation.

Next, the mass flow rate is defined as:

$$\dot{m} = \frac{C_d A_{orifice}\sqrt{2\bar{\rho}}}{\sqrt{PR_{loss}(1-(\frac{A_{orifice}}{A})^2)}} \frac{\Delta p}{(\Delta p^2 + \Delta p_{crit}^2)^{1/4}} \tag{2.7}$$

Where C_d is the discharge coefficient, $A_{orifice}$ represents instantaneous open area, $\bar{\rho}$ is the average fluid velocity, and PR_{loss} is the pressure loss due to the decrease in cross-sectional area which is 1. Δp_{crit} is the pressure difference related to critical Reynold's number.

2.2.3 Centrifugal Pump (IL)

Centrifugal pump (Iso-thermal) is the most important component in this simulation circuitry. Similar to the physical pump converting electrical power provided by the drive motor in figure 1.1, centrifugal pump (IL) converts the power provided by the velocity source from the mechanical rotational circuitry (R & C ports) to isothermal liquid circuitry (A & B ports) as shown in figure 2.5. Iso-thermal, written as IL, means that the operating environment is at constant liquid temperature. This component assumes the head of the pump is due to static pressure instead of dynamic pressure. Also, it is created by using Affinity Law, namely Similarity Laws in the lab manual [17], where characteristics of the pump such as torque, head, and flow rate can be predicted by using the ratio with respect to the referenced shaft speed values as shown in equations below.

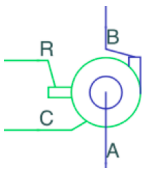

Figure 2.5. Centrifugal pump (IL)

According to the MathWorks documentation [20], the pressure difference across port A and B is defined as:

$$p_A - p_B = \Delta H_{ref} \rho g (\frac{\omega}{\omega_{ref}})^2 (\frac{D}{D_{ref}})^2 \tag{2.8}$$

Where g is the gravitational acceleration, ΔH_{ref} is the reference pump total head where pump efficiency at maximum, ω is the shaft velocity, which is also the input of this simulation, ω_{ref} is the referenced shaft speed, $\frac{D}{D_{ref}}$ is assumed to be 1 in this case since the system pump in the simulation should be equivalent to the referenced pump.

Similarly, the shaft torque is defined as:

$$\tau = W_{brake,ref} \frac{\omega^2}{{\omega_{ref}}^3} (\frac{D}{D_{ref}})^2 \tag{2.9}$$

Where $W_{brake,ref}$ is the referenced brake power at given shaft speed, and it is defined as:

$$W_{brake,ref} = \frac{q_{ref} \Delta H_{ref}}{efficiency_{max,ref}} \tag{2.10}$$

Where $efficiency_{max,ref}$ is the max efficiency reference point, and q_{ref} is the flow rate reference point at max pump efficiency. q_{ref} is defined as:

$$q_{ref} = \frac{\dot{m}}{\rho} \frac{\omega_{ref}}{\omega} (\frac{D_{ref}}{D})^3 \tag{2.11}$$

All equations above are the core mechanics for the analytical parameterization of centrifugal pump (IL), the reason is discussed in the implementation section.

2.3 Principle of Experiment & Governing Equations:

Apart from the MathWorks equations, the governing principles as well as the characteristics equations of the centrifugal water pump from the real experiment are described as follows:

The pump is analyzed theoretically based on the principles of modified Bernoulli's equation while accounting for the effect of friction as shown in equation 2.12.

$$H - h_f = \frac{\Delta P}{\rho g} + \left(\frac{V_2^2}{2g} + Z_2\right) - \left(\frac{V_1^2}{2g} + Z_1\right) \tag{2.12}$$

Where ΔP, V and Z are the pressure difference, velocity, and height of the liquid across the inlet (Z_1) and outlet (Z_2) of the pump. Utilizing this equation carries certain assumptions inherent in a Bernoulli system [22]: no heat transfer, no leaks, steady flow, incompressible, total pressure constant along streamline, and no energy loss.

To calculate pump efficiency, the Water Horsepower (WHP) and the Shaft Horsepower (SHP) should be obtained as shown with equation 2.13 and 2.14.

$$WHP = Q\rho gH \tag{2.13}$$

$$SHP = \omega T \tag{2.14}$$

In equation 2.13, Q is the volumetric flow rate of liquid, ρ is the liquid density, g is the acceleration of gravity on earth, and H is the total pump head. In equation 2.14, ω is the shaft angular velocity and T is the shaft torque. The pump efficiency is the ratio of WHP and SHP [21], as shown in equation 2.15.

$$\eta = \frac{WHP}{SHP} \tag{2.15}$$

Lastly, the water pump module is carefully configured using the actual laboratory data gathered from the physical device. By calculating the total head with equation 2.12, the result for head reference along with recorded values for flow rate as well as brake power reference will become the input for the pump.

2.4 Implementation of MATLAB SimScape Modules:

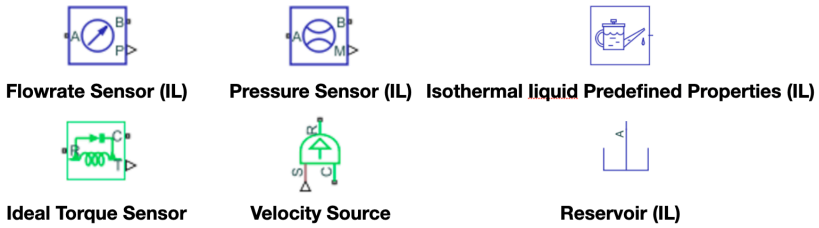

Figure 2.6. Additional components

Thus, major components including centrifugal water pump (IL) as shown in figure 2.5, pipe (IL) in figure 2.3, and orifice (IL) in figure 2.4, are implemented to the circuitry as shown in figure 1.2. Using the Isothermal Liquid Predefined Properties (IL) and Reservoir (IL) from figure 2.6, the liquid properties such as temperature, pressure, and density are settled. To initiate the flow, velocity source that directly links to a given shaft speed value

(in RPM) will give power to the water pump. To measure the liquid flow rate, pressure drop across the pump, and the torque readings for the pump, Flowrate Sensor (IL), Pressure Sensor (IL), and Ideal Torque Sensor are implemented into the circuit. However, for the torque sensor and pressure sensor, some calibrations must be implemented to take the realistic friction loss, viscous effect, etc. into account. Considering the fact that Centrifugal Pump (IL) is built based on the Affinity Law that only considers the ideal case, the curve fitting of the results in realistic scenarios.

2.4.1 Pros and Cons of Three Methods for Pump Parameterization:

As mentioned in section 2.2.3, centrifugal pump (IL) has multiple ways to parameterize the pump: analytical parameterization, 1D tabulated data parameterization, and 2D tabulated data parameterization, and the methods are discussed below.

2.4.1.1 Analytical Parameterization:

Analytical method requires sets of inputs that include capacity (flow rate), total head, and brake horsepower at a referenced shaft speed.

2.4.1.1.1 Pros of Analytical Parameterization:

This method only takes three sets of referenced values when the flow rate is at 0, when the total head is at maximum, and when the pump efficiency is at maximum, a total of 3 sets of data points. Hence, it is very easy to configure as shown in figure 2.7.

2.4.1.1.2 Cons of Analytical Parameterization:

This method is not very accurate, unless the reference data from physical pump are accurately collected. In addition, the pump characteristics are estimated using the curve fitting among the reference data, so the values from the curve fitting may not depict well for the actual pump characteristic from physical laboratory.

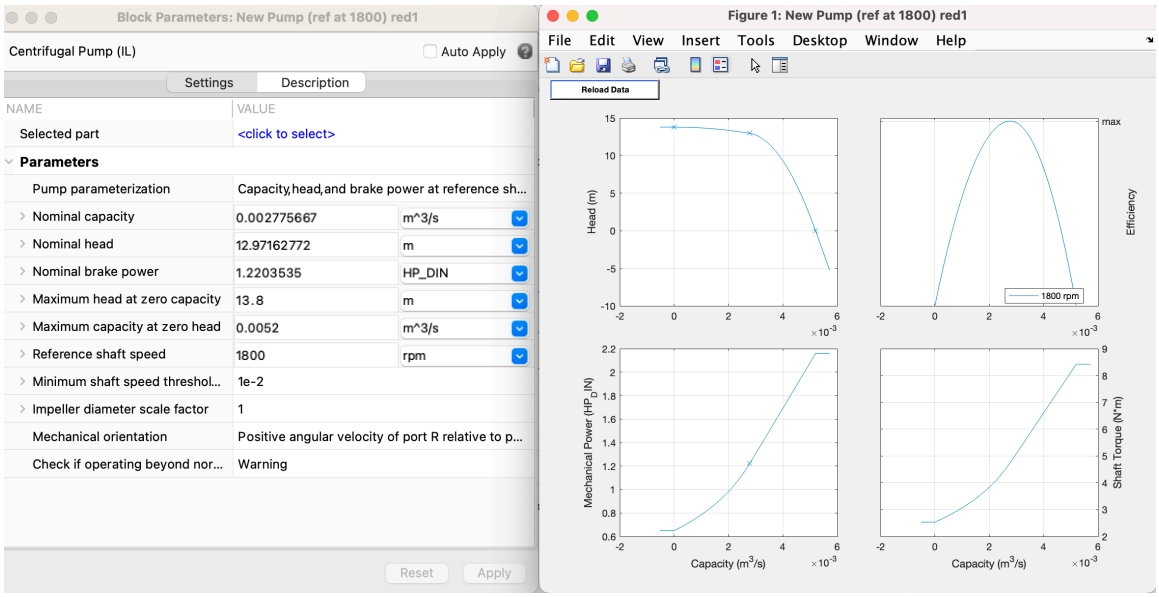

Figure 2.7. Centrifugal pump – example of analytical parameterization

2.4.1.2 1D Tabulated Data Parameterization:

1D parameterization method requires flow rate, total head, brake horsepower in the vector form that accurately depicts the characteristic of the pump at a referenced shaft speed.

2.4.1.2.1 Pros of 1D Tabulated Data Parameterization:

This method can be relatively accurate if enough data points are taken for the reference (figure 2.8) since the pump uses affinity law to predict results at different shaft speed.

2.4.1.2.2 Cons of 1D Tabulated Data Parameterization:

The disadvantage of this method is that the data has to be either in decreasing or increasing order for flow rate, total head, and brake horsepower. It means that any fluctuation from the physical data collection is unacceptable, making this method eventually lean towards the analytical prameterization but with more time wasted during the configuration process.

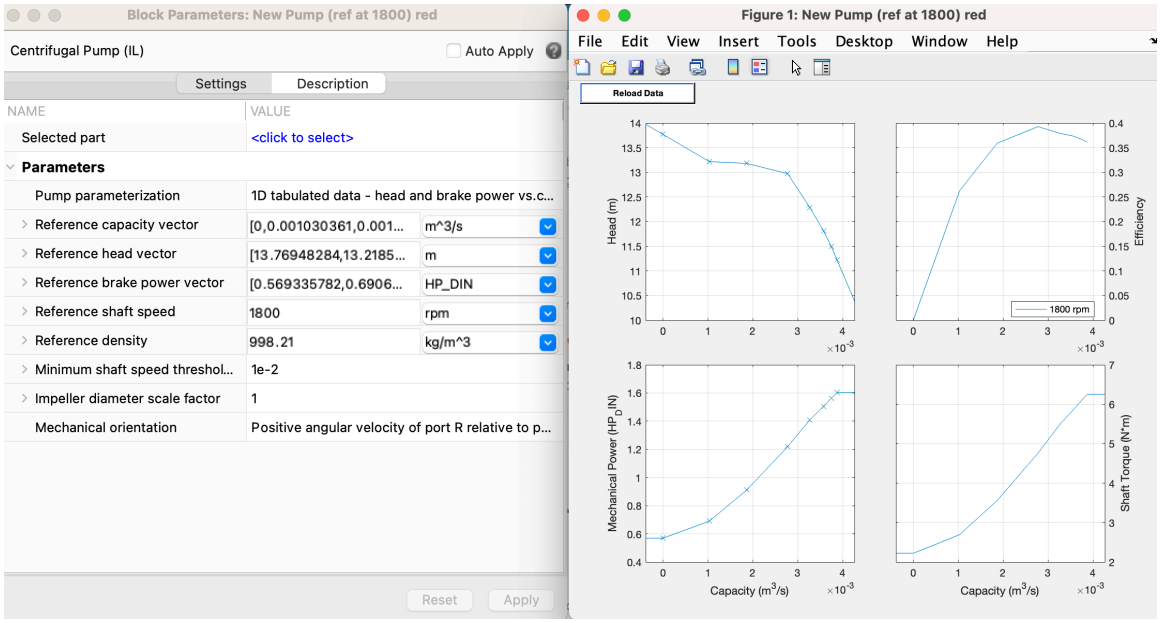

Figure 2.8. Centrifugal pump – example of 1D parameterization

2.4.1.3 2D Tabulated Data Parameterization:

The 2D parameterization method requires shaft speeds, flow rate, total head, brake horsepower in the vector form that accurately depicts the characteristic of the pump.

2.4.1.3.1 Pros of 2D Tabulated Data Parameterization:

This method is theoretically the most accurate method comparing to the other two, since it has extra reference curves at multiple shaft speeds as shown in figure 2.9.

2.4.1.3.2 Cons of 2D Tabulated Data Parameterization:

Given the pumps from the physical experiment, it is quite difficult to get all referenced values within the same flow rate domain among different pump shaft speed. For example, in the figure 2.9 where data is gathered from 1200, 1500, and 1800 RPM, the flow rate domain starts from 0 to roughly 0.002 $\frac{m^3}{s}$. That is smaller than the scale in figure 2.7 and 2.8 where at referenced shaft speed 1800 RPM, the flow rate domain starts from 0 to roughly 0.004 $\frac{m^3}{s}$. That is, to accommodate more different shaft speeds, the flow rate scale has to be adjusted to match the minimum shaft speed. Doing so leadsthe data points beyond the defined flowrate limit which is hard to predict, because the results are outside of the curve.

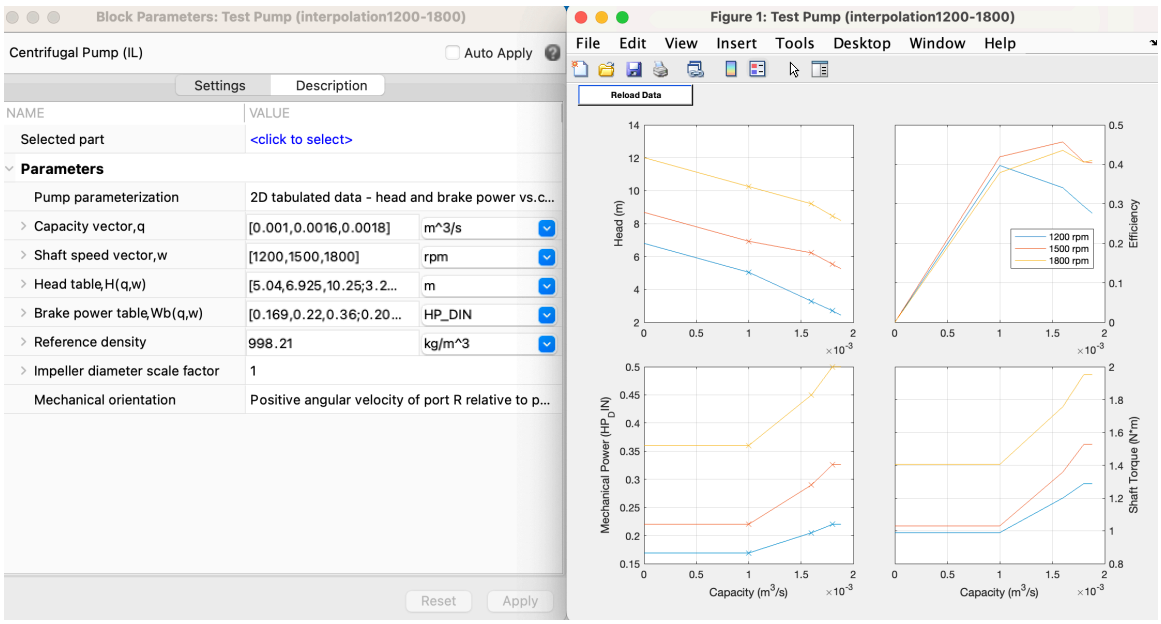

Figure 2.9. Centrifugal pump – example of 2D parameterization

The measurement error as discussed in Section 1 is implemented for three sensor values. However, before doing so, the model has been tested with varying the shaft speed from

1800 RPM to 300 RPM to verify the simulation, which is the same procedure as in Lab Manual Part 2. Strangely, it can be spotted that as the shaft speed decreases as shown in figure 2.10, which is represented by decrease in flow rate, the efficiency increases despite the fact that it should be decreasing in a real experiment. According to equation 2.15, the efficiency is the ratio of WHP and SHP, which are also directly proportional to the total head and torque values. Note that the Centrifugal Pump (IL) also follows the Affinity Law where according to equation 2.8, 2.9, 2.10, and 2.11, the head, torque, and flow rate all correlates to the ratio of input shaft speed and referenced shaft speed. Thus, it is reasonable to believe that the Centrifugal Pump (IL) directly using the ideal Affinity Law fails to accurately predict the efficiency at different shaft speeds, but is relatively accurate for the flow rate at those conditions.

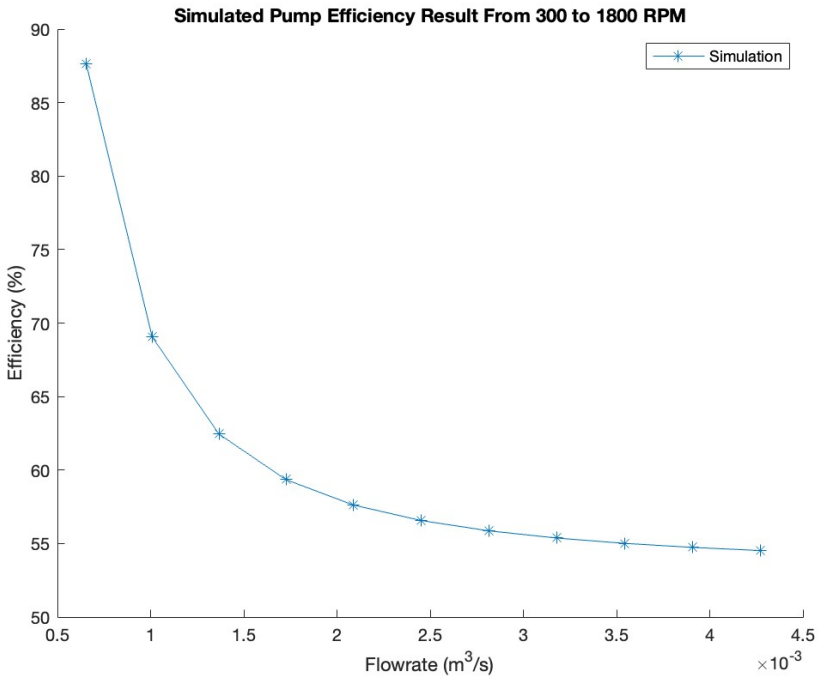

Figure 2.10. Uncalibrated pump efficiency curve (same trend for both pumps)

To remedy the effect due to the difference, which also reflects previously ignored water viscous effect, inertial force, and other frictional loss that have not yet been considered in this model, curve fitting for torque and pressure readings have been implemented as shown in figure 2.11, 2.12, 2.13, and 2.14. Y-axis of the plot is the difference in simulation and experimental readings. To make sure the simulation readings do not overfit against the part 2 results, the difference is taken only at shaft speed 300, 600, 900, 1200, 1500, 1800 RPM.

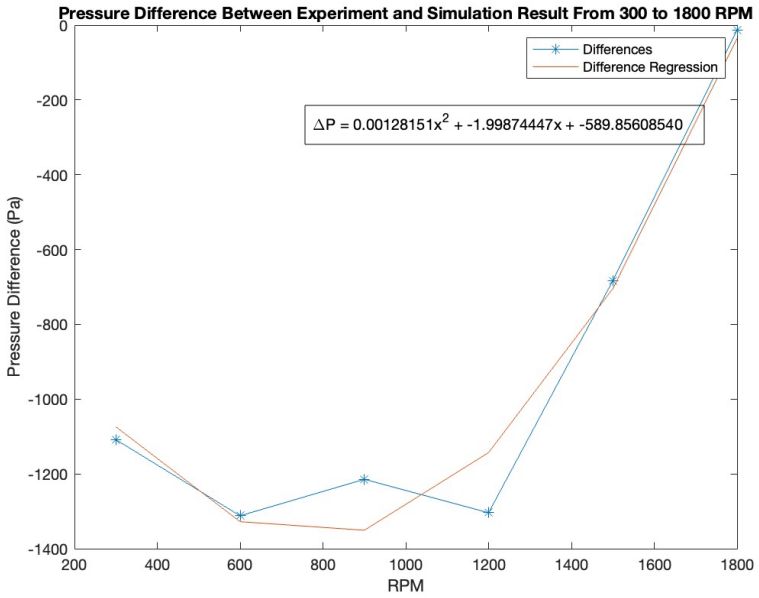

Figure 2.11. Fitting curve for pressure difference of gold pump

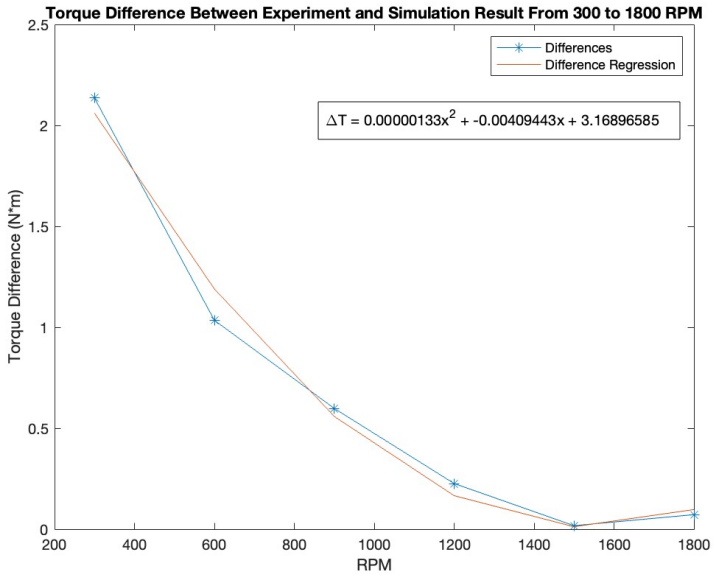

Figure 2.12. Fitting curve for torque difference of gold pump

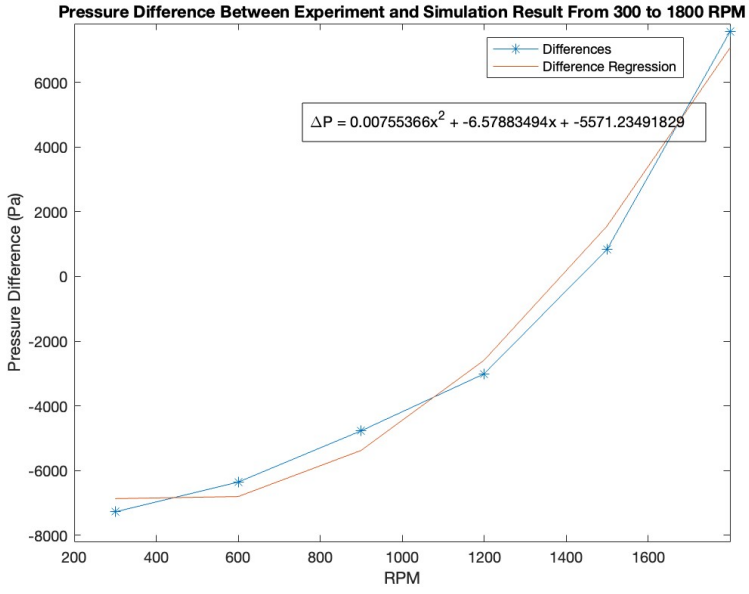

Figure 2.13. Fitting curve for pressure difference of red pump

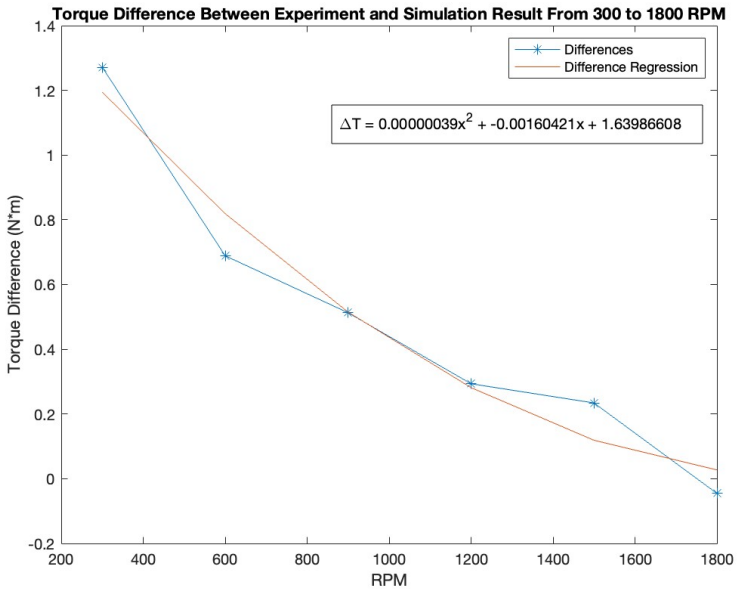

Figure 2.14 Fitting curve for torque difference of red pump

After using 2nd order curve fittings and carrying the polynomial factors into the pressure sensor and torque sensor circuitry, respectively, as shown in figure 2.15, 2.16, 2.17, the measurement error can now be implemented using random number generator (followed normal distribution) ranges ± 0.5% of the output readings after calibration as shown below.

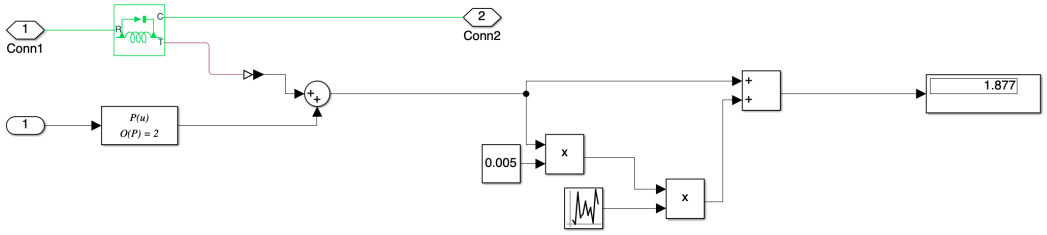

Figure 2.15. Uncertainty circuitry for torque result (both pumps)

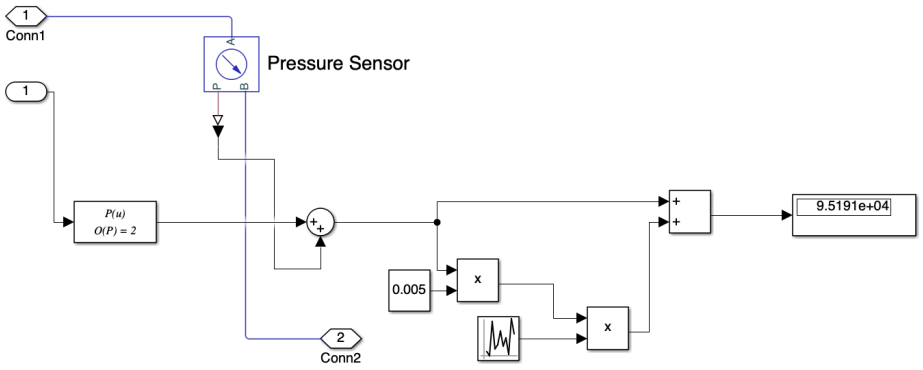

Figure 2.16. Uncertainty circuitry for pressure result (both pumps)

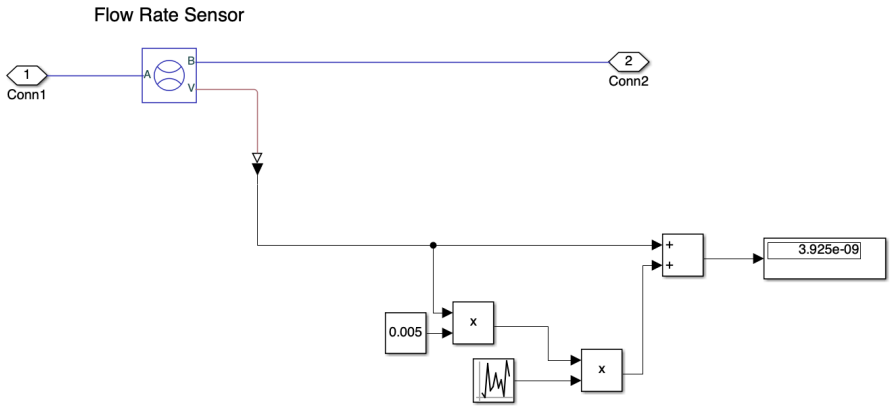

Figure 2.17. Uncertainty circuitry for flow rate result (both pumps)

As for the reason to implement uncertainty factors, the physical model of the water pump is constructed based on numerous PID (Proportional-Integral-Derivative) control loops [15], which means that the physical water pump will continuously output results such as pressure drops, torque, etc., trying to reach the minimized error between the measure value and desired value. Such process will cause fluctuations as the controller keeps seeking the most accurate result, and sometimes results can be unstable or time-consuming for a steady state. Thus, most errors from the original device arise not only from measurement inaccuracies and sensor discrepancies but also from the inherent fluctuations in PID

readings due to various response time. Hence, noise generator as shown in figure 2.15, 2.16, and 2.17 is utilized in this simulation as the source of measurement error. This approach effectively replicates the uncertainty encountered during actual experiments, and more detailed comparison between experiment results and simulation results will be discussed in chapter 3. Before addressing the result section, the right choice of parameterization with Centrifugal Pump (IL) must be decided.

2.4.2 Attempts & Final Selection for Pump Implementation Method:

All three methods of parameterizing the pump haven been tested. Based on their pros and cons, only one method is selected for the final simulation model.

Start with the 2D parameterization, since it has the most accurate approximation. The solution to remedy the inaccuracy of data points beyond the threshold of the flow rate is to parameterize the shaft speed with a closer range of values. For example, 1500 to 1800 RPM. However, students will need to measure the pump characteristic from 300 to 1800 RPM, so there will be more than one defined pump in the simulation circuitry, i.e., 300 to 600, 600 to 900, etc. In addition, more parameterizations require more time to record the values, and requires the physical pump to provide stable results that can be taken as inputs. Unfortunately, both pumps cannot provide stable results at low RPM region, and this shall be discussed in the next section.

The 1D Parameterization is a reasonable route, but it shares similar disadvantage as in 2D Parameterization. First, the data recorded must be accurate and contain as many points as possible to depict accurate characteristic curves. Second, the physical pump, especially the newer one with red impeller, sometimes undergo software updates that may change the flow rate and pressure sensor reading, leading to further variances to flow rate and total head curves as where data gathered by students in each year has great differences, making parameterization process harder to finalize the reasonable input.

Therefore, this simulation is built upon the Analytical Parameterization as in figure 2.18, because it is easy to configure and relatively accurate to depict the ideal pump characteristic curves.

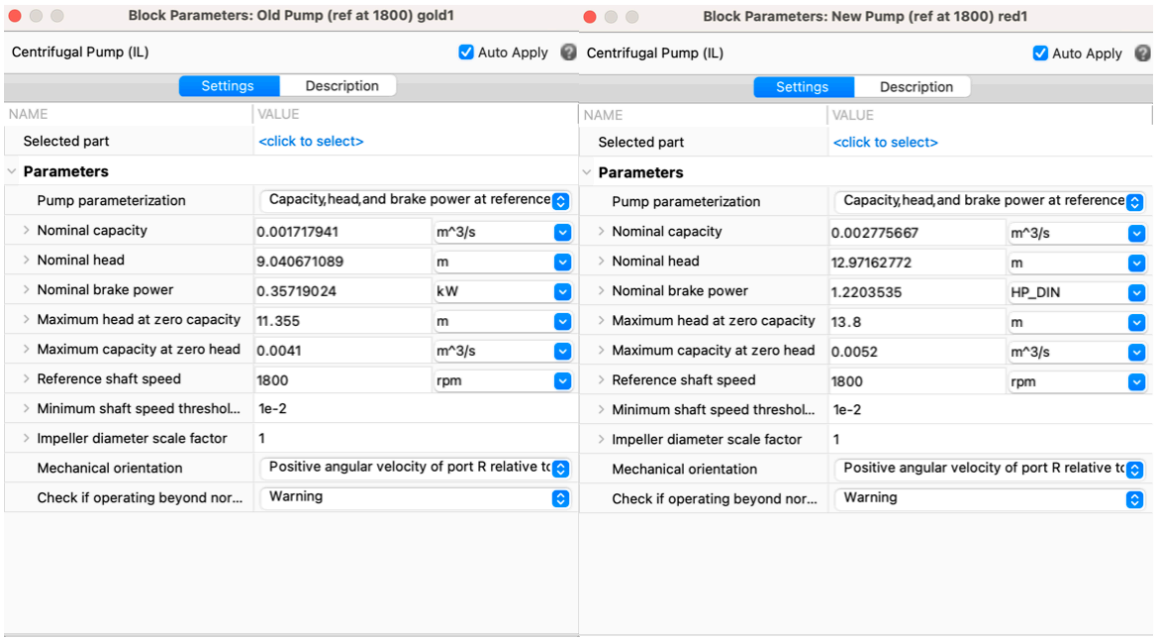

Figure 2.18. Final Pump Selection & Configuration for Pump with Red (Right) and Gold (Left) Impeller

CHAPTER 3

RESULTS AND DISCUSSION

This chapter will mainly fulfill the validation process of the simulation model, and further discusses the impact from parameters setup. It covers in-depth comparison between simulation and experiment results, data analysis from conducting virtual and physical experiments, as well as the criteria of becoming a digital twin for physical water pump unit.

3.1 Simulation & Experiment Results Comparison:

As previously mentioned, the built-in SimScape modules have been verified by MathWorks, and the piping design can be referred to the textbook as mentioned in the previous section. Therefore, comparison test between the simulation model and the physical unit can now be conducted for the validation process.

The characteristics being compared for the pumps are the total head, Water Horse Power (WHP), Shaft Horse Power (SHP), and efficiency at chosen shaft speeds. Those shaft speeds include 300, 600, 900, 1200, 1500, 1800 RPM. Additionally, there is a case with constant increase in shaft speed from 300 to 1800 RPM, with each step incrementing by 150 RPM. Also, for the visual consistency of the comparison test, the test is conducted following the same steps of the experiment part 1 and part 2 as described in the lab manual [17]. That is, recording eleven data points at gate valve from maximum opening to fully closed position, closing the valve two turns each step in a total of 20 turns. To evaluate the performance and accuracy between the models, detailed pump characteristic curves are

analyzed by using statistical tests such as Mean Absolute Error (MAE), Root Mean Squared Error (RMSE), as well as Coefficient of Determination (R^2).

MAE, as shown in equation 3.1, presents the error by using the absolute difference between each simulation value and corresponding experiment value, summing up those absolute differences, then dividing by the sample amounts.

$$MAE = \frac{1}{\#\ of\ samples} \sum_{i=1}^{\#\ of\ samples} |simulation - experiment| \qquad (3.1)$$

RMSE, as shown in equation 3.2, measures the error using the square of the differences between each simulation value and its corresponding experiment value, then calculating the square root of the summed up the differences that has been divided by the sample amounts.

$$RMSE = \sqrt{\frac{1}{\#\ of\ samples} \sum_{i=1}^{\#\ of\ samples} (simulation - experiment)^2} \qquad (3.2)$$

The Coefficient of Determination (R^2), as shown in equation 3.3, depicts a proportion of variance that indicates how predictable are experiment results based on simulation results.

$$R^2 = 1 - \frac{\sum(experiment - simulation)^2}{\sum(experiment - average\ of\ experiment)^2} \qquad (3.3)$$

These statistical tests follow rigorous rules. The first rule is that the sample sizes of both experiment and simulation must be the same. This is a hindrance since the original

laboratory unit, especially the pump with red impeller, requires users to collect data points with an input time interval. The process starts with a mouse click and ends with the final one, thus being extremely difficult to gather data point individually. The second rule is that data points being compared between simulation and experiment must be aligned at the same dimension and same scale. In this instance, they must have the same flowrate in order for the comparison to proceed.

Therefore, the approach to resolve this issue involves two steps. First, each clustered data points resulting from the recording method of the pump with red impeller must be averaged out to the closest reasonable flowrate, and the process must ensure that there are enough data points for the comparison analysis. Second, using interpolation method to find the corresponding characteristic values from experiment dataset given the simulation flowrate, because doing so will align the data points between simulation and experiment results at the same corresponding flowrates to meet the standard of statistical tests.

In addition, all results regardless of simulation or experiment have been applied with uncertainties. As mentioned before, the total uncertainty is affected by both bias and precision uncertainty. The bias uncertainty and precision uncertainty calculation will be further discussed in the next few sections. The uncertainty calculation steps can be referred to Appendix B, and it will also be analyzed in the later sections.

After gathering the corrected data, the validation process can proceed. Further details are discussed in the next section.

3.1.1 Comparison at 1800RPM

In the figure 3.1 and 3.2, the total head and WHP at shaft speed of 1800 RPM are compared for both pumps. Judging by the MAE and RMSE, both simulation models depict the experimental total head and WHP very well. As for the $\boldsymbol{R^2}$ values, the pump with red impeller is relatively low, indicating that there are inaccuracies in predicting the experiment results based on the simulation ones. The potential reason could be due to the inaccurate nominal point during the parameterization process, because the Pump (IL) which follows analytical parameterization records three reference points as discussed before. Thus, the simulated total head curve may only consider the ideal case whereas the realistic total head curve undergoes dynamic fluctuations and possibly experiment errors. Nevertheless, the issue has minimal impact on depicting the general trend as well as the overall result, as the WHP is only slightly affected in the comparison of pump with red impeller.

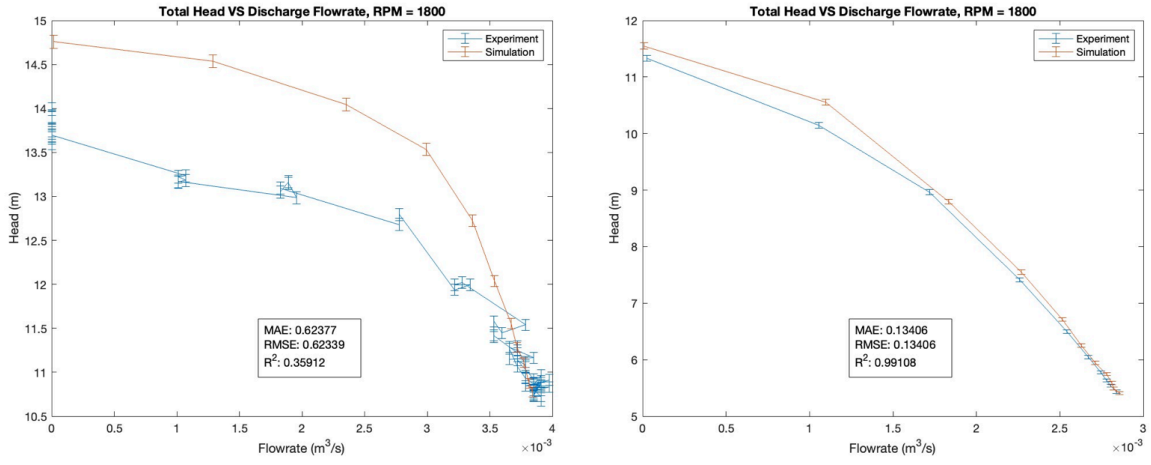

Figure 3.1. Total head vs discharge fowrate for the pump with red (left) impeller and gold (right) impeller at 1800 RPM

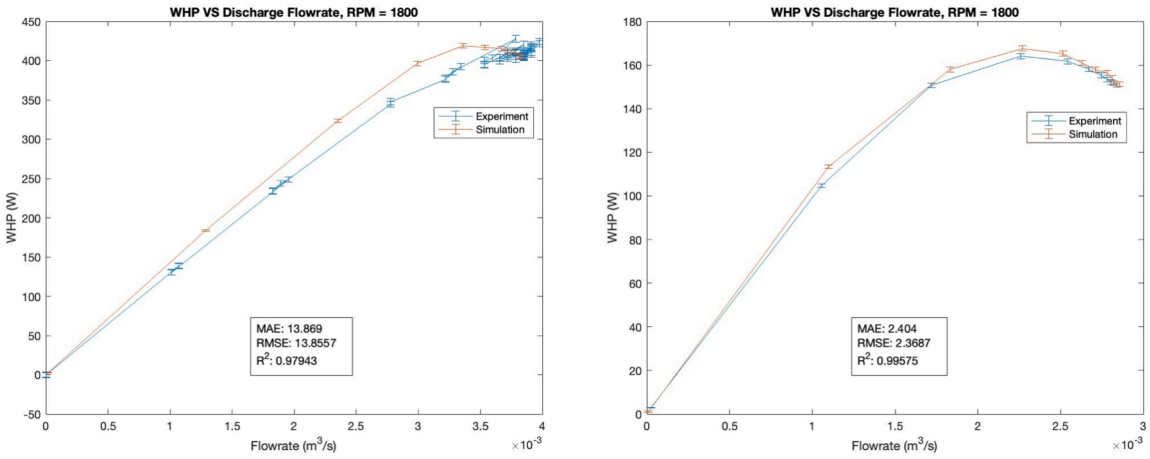

Figure 3.2. WHP vs discharge flowrate for the pump with red (left) impeller and gold (right) impeller at 1800 RPM

From figure 3.3, both pumps provide relatively close SHP between simulation and experiment supported by all three statistical criteria. However, it can be noticed that the simulation SHP curve starts to diverge from the experimental one as the flowrate decreases to a certain value, which is around $2.5\text{x}10^{-3}\ \frac{\text{m}^3}{\text{s}}$ for pump with red impeller and $1.75\text{x}10^{-3}\ \frac{\text{m}^3}{\text{s}}$ for pump with gold impeller. This is caused by the method of Analytical Parameterization, which only considers three input points to describe the curve. While the issue could potentially be addressed with 1D and 2D Parameterization, it is important to note, as mentioned earlier, that increasing the number of inputs will require as many rigorously precise recorded values as possible from the physical device to generate the perfect curve.

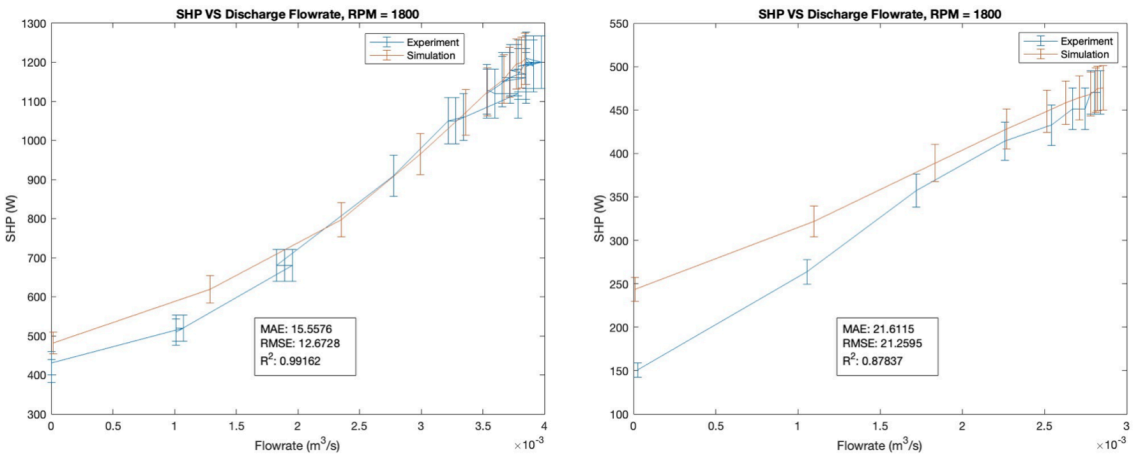

Figure 3.3. SHP vs discharge flowrate for the pump with red (left) impeller and gold (right) impeller at 1800 RPM

From figure 3.4, the pump with red impeller presents acceptable efficiency results that meet the criteria compared with the experiment ones. Interestingly, the discrepancies spotted earlier in total head, WHP, and SHP eventually cancel out each other in the resulting efficiency curve. Still, the differences existed in the total head affects the WHP, leading to a slightly higher efficiency of 40% around $2.75\text{x}10^{-3}\ \frac{m^3}{s}$ flowrate comparing to 38% efficiency in the experimental result. The pump with gold impeller also has similar trend and results comparing between simulation and experiment data sets. However, it is worth noticing the difference around a flowrate of $1.2\text{x}10^{-3}\ \frac{\text{m}^3}{\text{s}}$, where the efficiency deviates the most. The cause is obviously due to the simulation SHP value being larger than the experimental value, and the reason is due to the inaccuracy in method of Analytical Parameterization which has been mentioned previously.

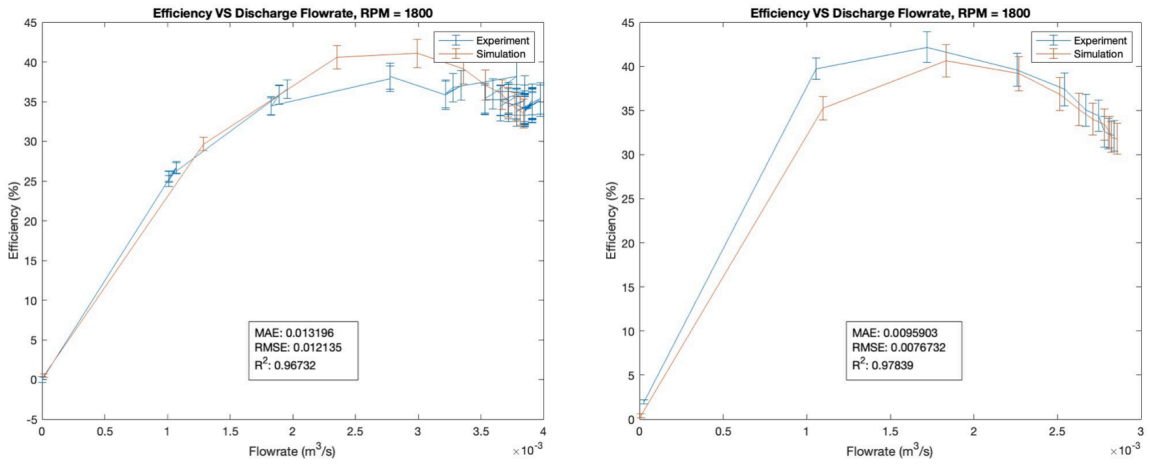

Figure 3.4. Efficiency vs discharge flowrate for the pump with red (left) impeller and gold (right) impeller at 1800 RPM

3.1.2 Comparison at 1500RPM

According to figure 3.5 and figure 3.6, the same discrepancies mentioned at a shaft rotational speed of 1800 RPM still persist in the total head and WHP curves with a rotational speed of 1500 RPM for the pump with red impeller, but the flowrate at which the total head and WHP diverge is smaller. It is also worth noticing that the trend of those two plots is similar to the trend at 1800 RPM. These findings can theoretically refer to the concept of Affinity Law, since the total head is directly proportional to the squared ratio of shaft speeds, WHP is proportional to the total head according to equation 2.13, and flowrate is directly proportional to the ratio of shaft speed. Still, a detailed analysis between Affinity Law and actual results will be discussed later. What's more, the R^2 value of the total head gets better for the pump with red impeller, meaning that the discrepancies are getting lower as the shaft speed decreases.

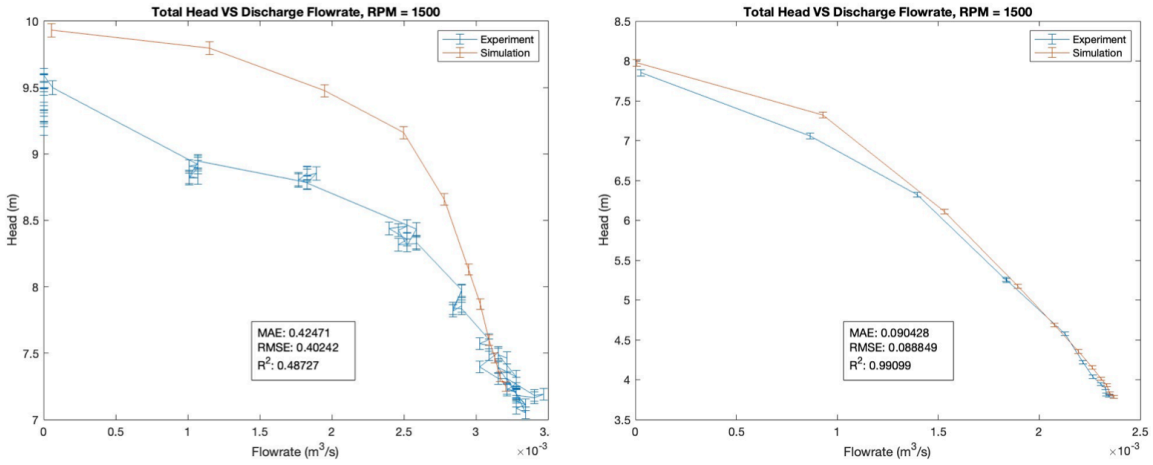

Figure 3.5. Total head vs discharge flowrate for the pump with red (left) impeller and gold (right) impeller at 1500 RPM

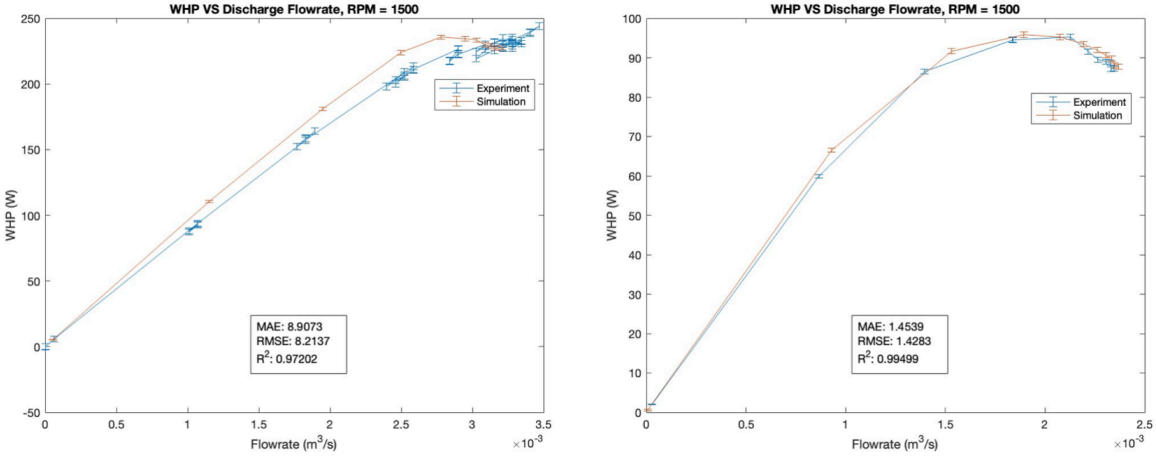

Figure 3.6. WHP vs discharge flowrate for the pump with red (left) impeller and gold (right) impeller at 1500 RPM

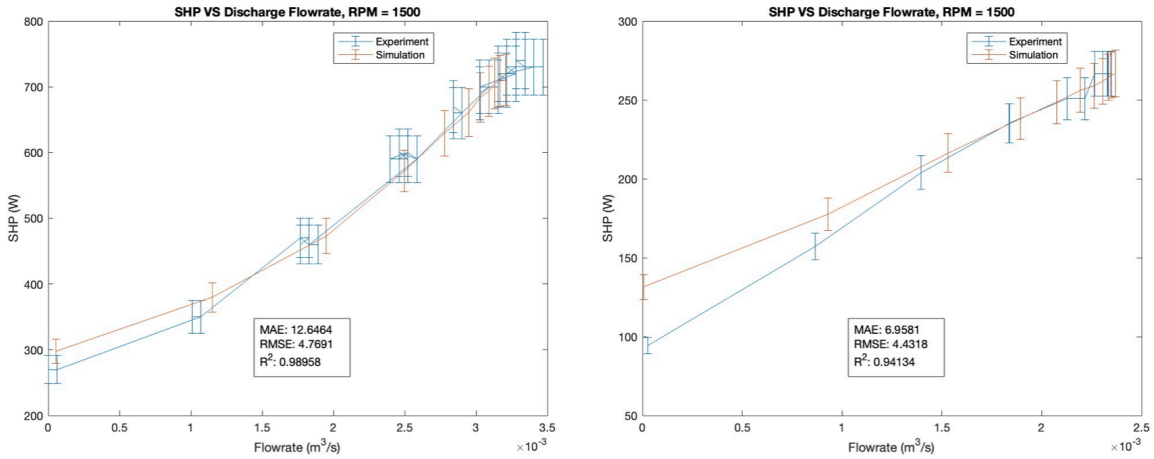

Figure 3.7. SHP vs discharge flowrate for the pump with red (left) impeller and gold (right) impeller at 1500 RPM

Similar trend can be spotted for SHP and efficiency curves as well according to figure 3.7, where SHP curves start to diverge around a flowrate of $1.35\text{x}10^{-3}\ \frac{\text{m}^3}{\text{s}}$ for the pump with gold impeller, and a flowrate of $1.5\text{x}10^{-3}\ \frac{\text{m}^3}{\text{s}}$ for the pump with red impeller. It can be also found that the discrepancies between SHP simulation and experimental values for both pumps are getting smaller comparing to the previous 1800 RPM case.

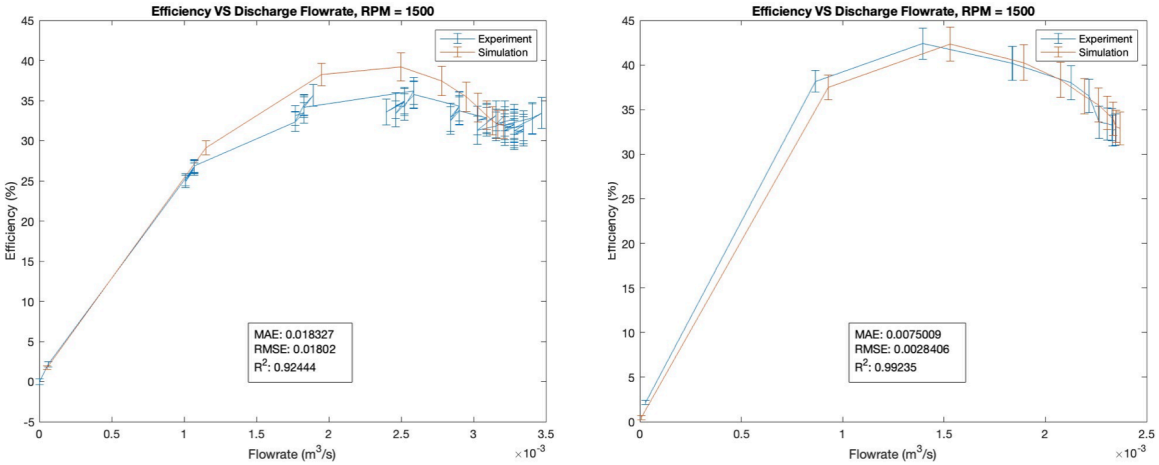

Figure 3.8. Efficiency vs discharge flowrate for the pump with red (left) impeller and gold (right) impeller at 1500 RPM

From figure 3.8, the efficiency curve also carries the similar trend from the pump with a rotational speed of 1800 RPM. And as mentioned, the gap between simulation and experiment curves are getting smaller. It can also be seen that the simulation result for maximum flowrate of the pump with red impeller has a slightly smaller value compared to the original experiment data. The possible reason could again originate from the parameterizing process, and this issue could amplify the difference of maximum flowrate between simulation and experiment. Another possible explanation for the differences is the fluctuations in the original experiment dataset. This is because the physical pump with red impeller may take some time to stabilize the flow and its readings, during which the unstable data might be recorded.

3.1.3 Comparison at 1200RPM

From figure 3.9, 3.10, 3.11, and 3.12, the similar trend that is originated from the pump with a rotational speed of 1800 RPM continues, and this time gaps between simulation and experiment result among all graphs stay relatively the same. As all figures start to show divergence at a flowrate of $\mathbf{1.5x10^{-3}}\ \frac{\mathbf{m^3}}{\mathbf{s}}$ for the red impeller, and $\mathbf{0.8x10^{-3}}\ \frac{\mathbf{m^3}}{\mathbf{s}}$ for the gold impeller. The discrepancy occurred at the maximum flowrate for the pump with gold impeller indicates the error made by curve fitting, bringing roughly 2% efficiency difference, which can be considered as a small error. As for the maximum flowrate difference of pump with red impeller, the difference is showing a decrease comparing to that in pump with a rotational speed of 1800 and 1500 RPM.

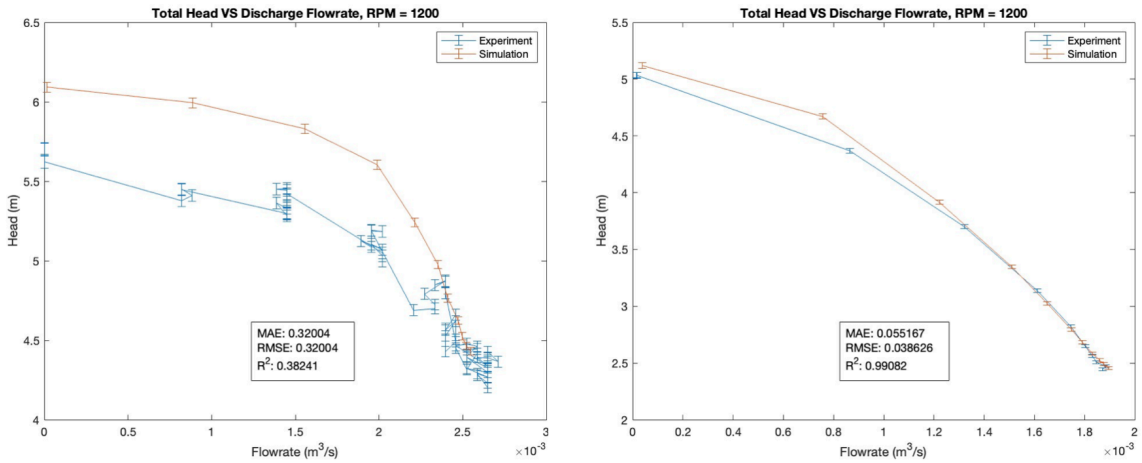

Figure 3.9. Total head vs discharge flowrate for the pump with red (left) impeller and gold (right) impeller at 1200 RPM

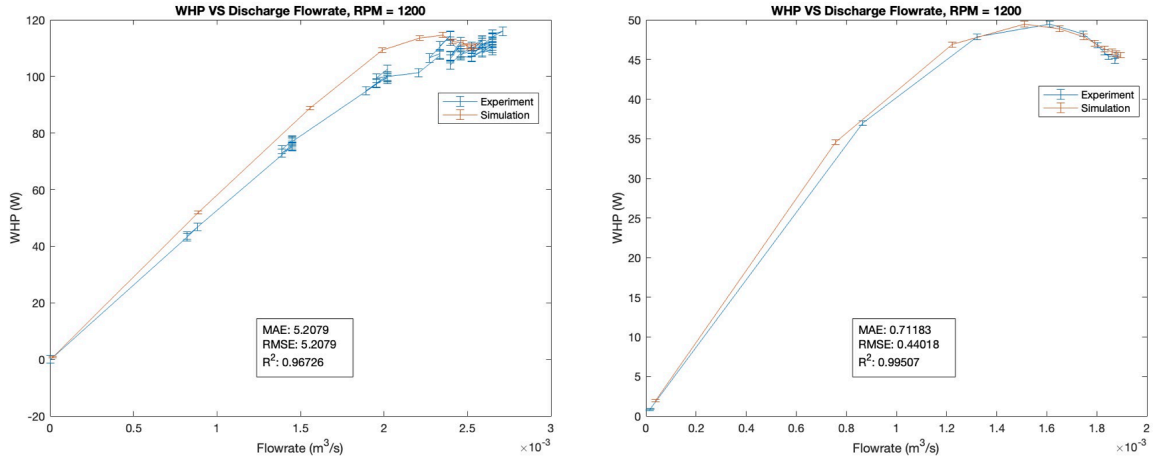

Figure 3.10. WHP vs discharge flowrate for the pump with red (left) impeller and gold (right) impeller at 1200 RPM

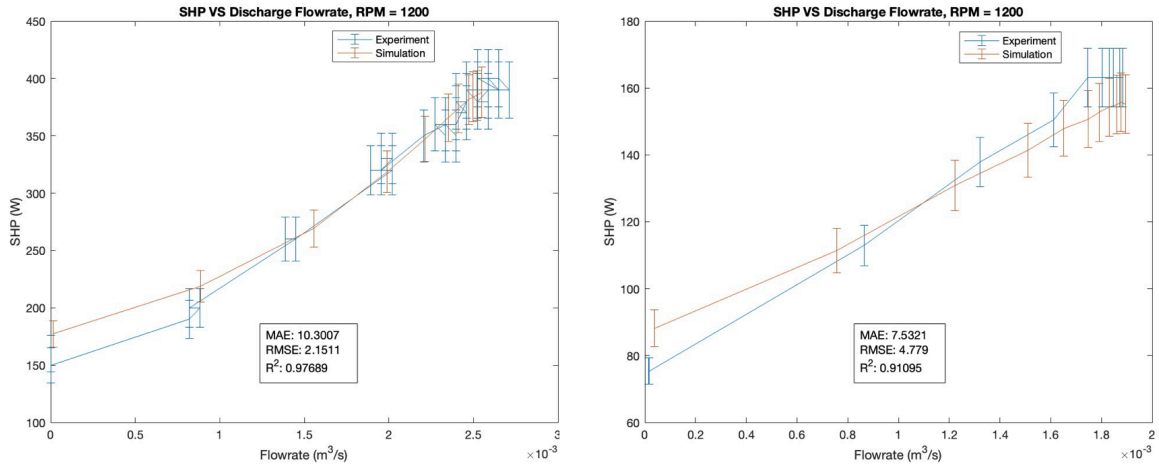

Figure 3.11. SHP vs discharge flowrate for the pump with red (left) impeller and gold (right) impeller at 1200 RPM

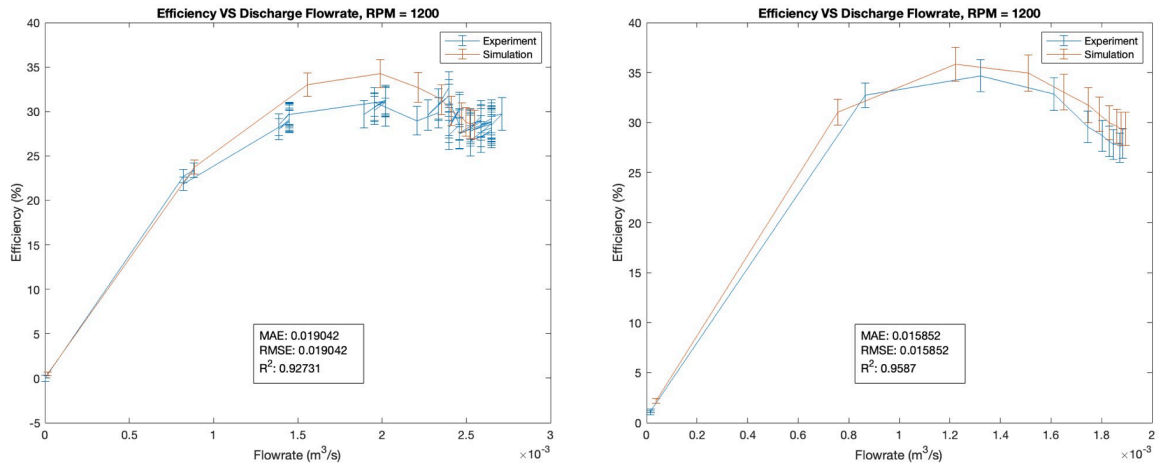

Figure 3.12. Efficiency vs discharge flowrate for the pump with red (left) impeller and gold (right) impeller at 1200 RPM

3.1.4 Comparison at 900 RPM

Based on aforementioned figures, both the total head and WHP curves demonstrate strong correlation between simulation and experiment curves for both pumps. It can be observed from both pumps, the statistical criteria for total head and WHP yield promising results

because both MAE as well as RMSE values are showing small numbers. Furthermore, the simulation curves from total head and WHP accurately mimic the evolution from experiment curves, and this can be seen from R^2 value which is close to 1.

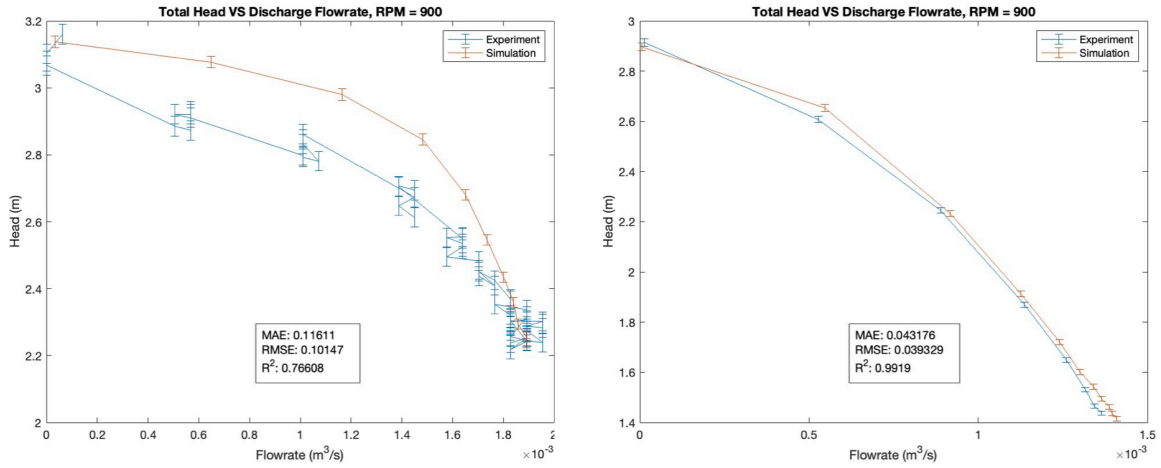

Figure 3.13. Head vs discharge flowrate for the pump with red (left) impeller and gold (right) impeller at 900 RPM

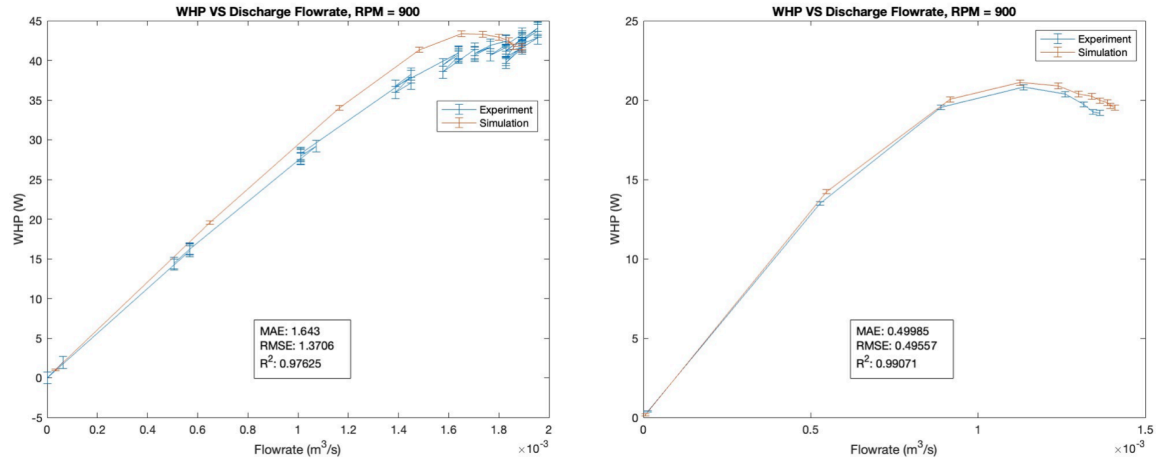

Figure 3.14. WHP vs discharge flowrate for the pump with red (left) impeller and gold (right) impeller at 900 RPM

From figure 3.15 and 3.16, the simulation and experiment SHP curve of the pump with red impeller return to be closely overlapped, despite the fluctuation generated in the experiment curve. As for the SHP of pump with gold impeller, the gap between simulation and experiment still remains. Still, efficiency results from simulation and experiment curves in both pumps show strong correlation to each other.

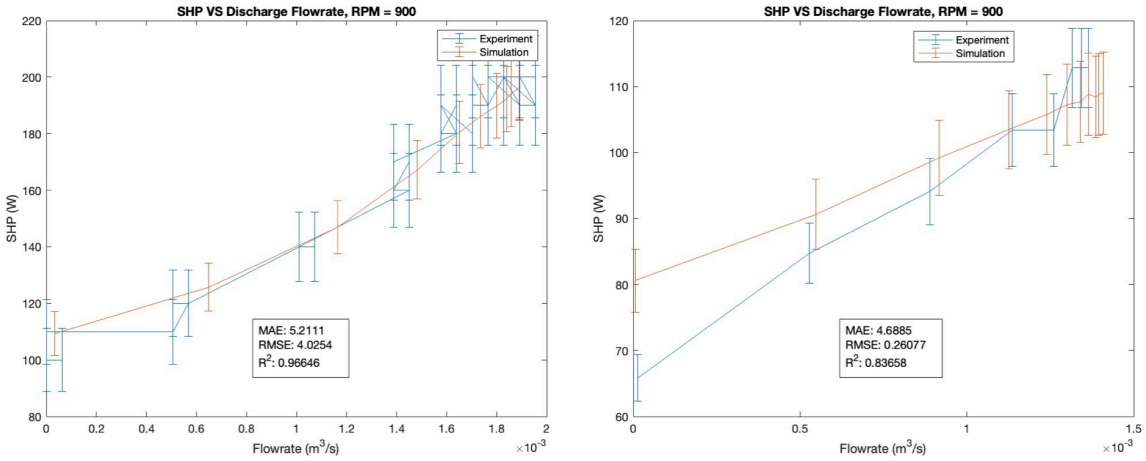

Figure 3.15. SHP vs discharge flowrate for the pump with red (left) impeller and gold (right) impeller at 900 RPM

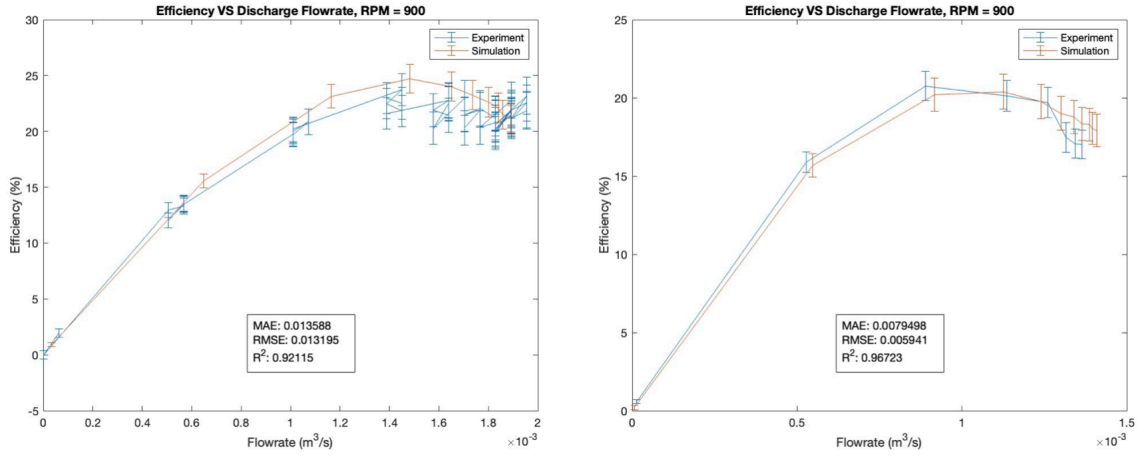

Figure 3.16. Efficiency vs discharge flowrate for the pump with red (left) impeller and gold (right) impeller at 900 RPM

3.1.5 Comparison at 600 RPM

From figure 3.17 and 3.18, though the correlation between simulation and experiment data in terms of total head and WHP for the pump with red impeller remains consistent as previous observations, the correlation for pump with gold impeller starts to show some divergence. Especially when the flowrate ranges from $0.35\text{x}10^{-3}\ \frac{\text{m}^3}{\text{s}}$ to $0.75\text{x}10^{-3}\ \frac{\text{m}^3}{\text{s}}$, there are variations between simulation and experiment result for both total head and WHP.

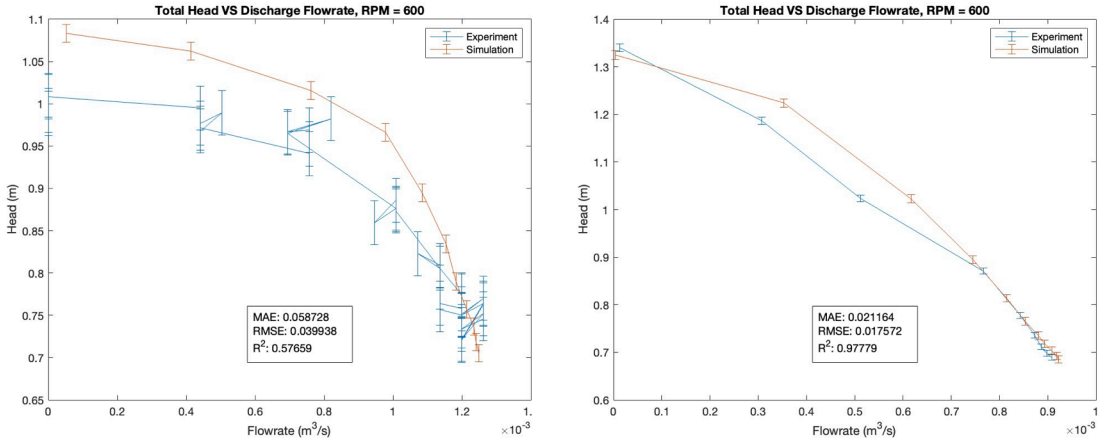

Figure 3.17. Total head vs discharge flowrate for the pump with red (left) impeller and gold (right) impeller at 600 RPM

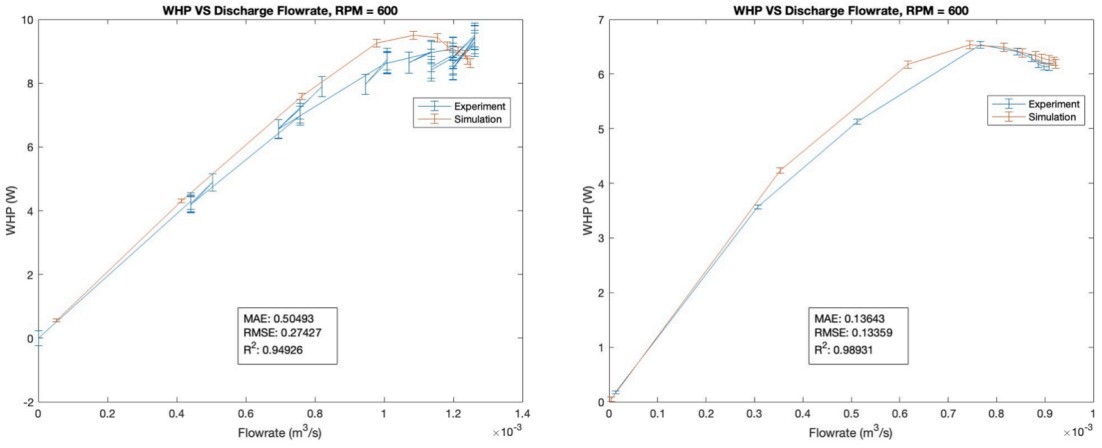

Figure 3.18. WHP vs discharge flowrate for the pump with red (left) impeller and gold (right) impeller at 600 RPM

From figure 3.17 and 3.18, though the correlation between simulation and experiment data in terms of total head and WHP for the pump with red impeller remains consistent as previous observations, the correlation for pump with gold impeller starts to show some divergence. Especially when the flowrate ranges from $0.35\text{x}10^{-3}\ \frac{\text{m}^3}{\text{s}}$ to $0.75\text{x}10^{-3}\ \frac{\text{m}^3}{\text{s}}$, there are variations between simulation and experiment result for both total head and WHP.

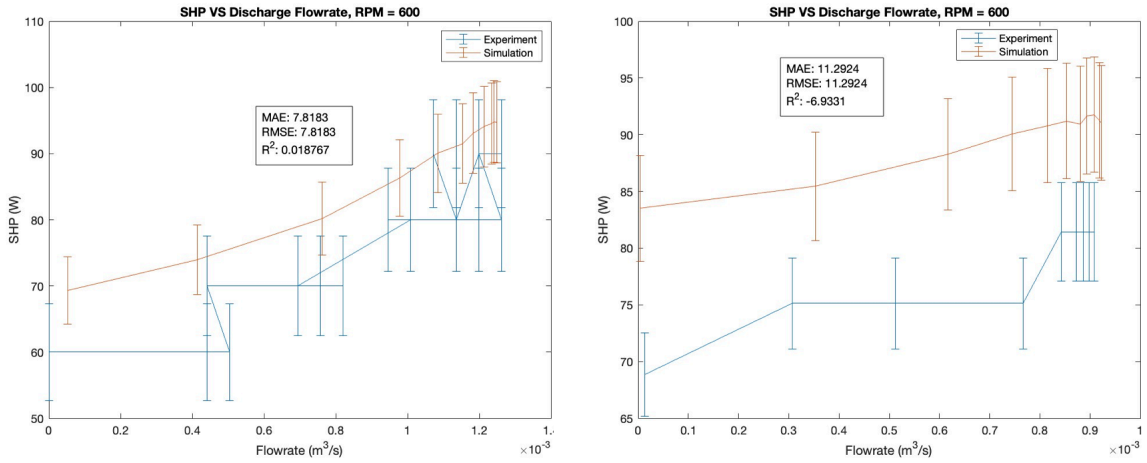

Figure 3.19. SHP vs discharge flowrate for the pump with red (left) impeller and gold (right) impeller at 600 RPM

From figure 3.19, the difference between simulation and experiment results in SHP can be seen in both pumps. Given that the difference between simulation and experiment curves remain consistent across all flowrates, it is reasonable to attribute the cause of such difference to the errors in calibration process.

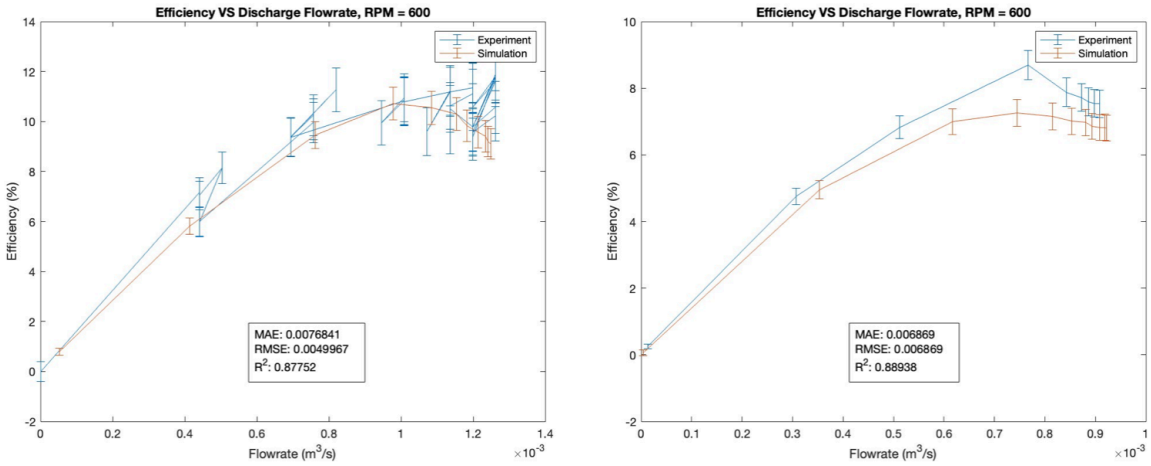

Figure 0.20. Efficiency vs discharge flowrate for the pump with red (left) impeller and gold (right) impeller at 600 RPM

From figure 3.20, the pump with red impeller has a fair correlated pairs between simulation and experiment, but the pump with gold impeller has a noticeable distinction at a flowrate of $0.35\text{x}10^{-3}\ \frac{\text{m}^3}{\text{s}}$ that is possibly due to curve fitting error.

3.1.6 Comparison at 300RPM

From figure 3.21, the large fluctuations as well as abnormal R^2 values suggest that the experiment total head results for both pumps lack stability. Especially for the pump with gold impeller, the flowrate experiences a substantial increase when the gate valve is closed to about 10 turns. Aside from that, results from the pump with red impeller has a negative total head value, indicating a backflow effect happened during the physical experiment. The detailed analysis on such phenomenon will be discussed in physical experiment section.

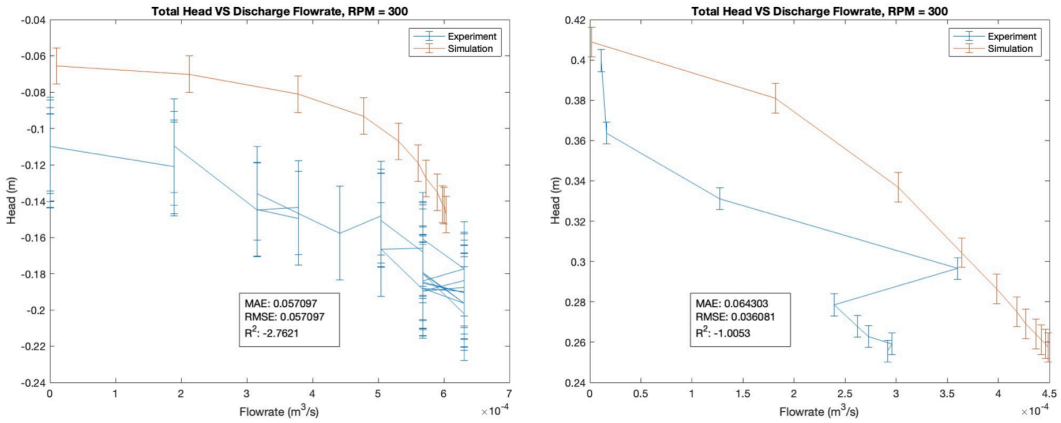

Figure 3.21 Total head vs discharge flowrate for the pump with red (left) impeller and gold (right) impeller at 300 RPM

From figure 3.22, the WHP follows the trend of the total head curves, which leads to a similar issue as seen in the Figure 3.21 for the pump with gold impeller, despite R^2 yielding a reasonable value. The experiment WHP for the pump with red impeller seems to be stable in terms of curvature. However, a negative R^2 value highlights the instability within the experiment data, and it is because the flowrate going back and forth, creating fluctuations in the experiment data. Meanwhile, both simulation curves still well define the WHP results, adhering to the Affinity Law and the curve fitting process.

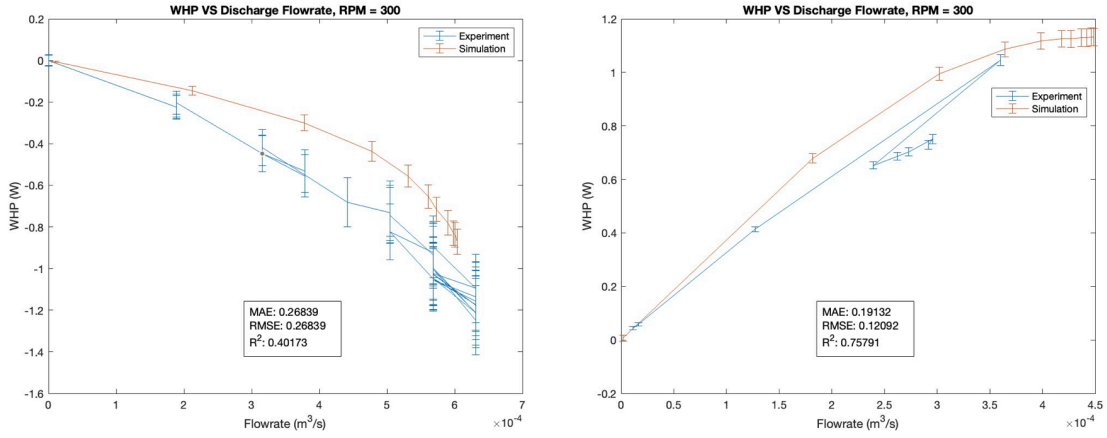

Figure 3.22. WHP vs discharge flowrate for the pump with red (left) impeller and gold (right) impeller at 300 RPM

From figure 3.23, both SHP plots exhibits considerable large discrepancies in terms of statistical tests and uncertainties. Especially for the distinct oscillation in the experimental data for both pumps. This can be explained by the design method employed in the physical laboratory unit, more specifically, the use of Proportional-Integral-Derivative (PID) control. At lower shaft speed, the response time of the system increases, causing the time to reach stability longer. Also, the water flow in the pipe may not be fully developed at lower shaft speed, especially right after the water flows through the bending portion of the pipe. What's more, the accuracy and resolution of sensors equipped on the physical unit might be lower at low flowrates, leading to the disturbances in the curves. The simulation not only does not take account for those effects from control theories, but also its piping setting criteria almost always provide laminar flow, resulting in relatively stable curves. As for the small fluctuations in the simulation curves, they are the results of the implementation of random noises as mentioned in the previous chapter.

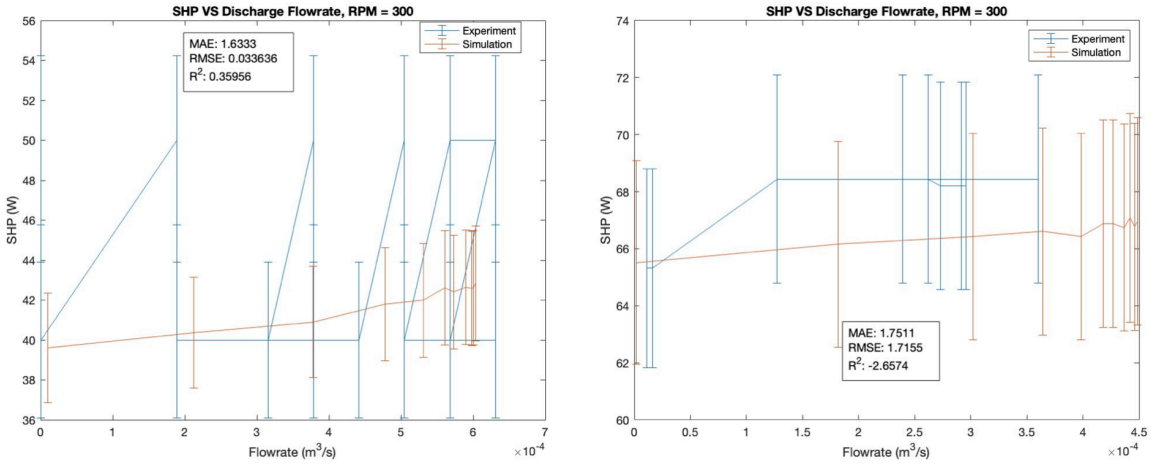

Figure 3.23. SHP VS discharge flowrate for the pump with red (left) impeller and gold (right) impeller at 300 RPM

From the figure 3.24, the experiment efficiency curves inherit both the fluctuations and trends from WHP and SHP curves. Meanwhile, the simulation efficiency curves persist in presenting the ideal case following the Affinity Law.

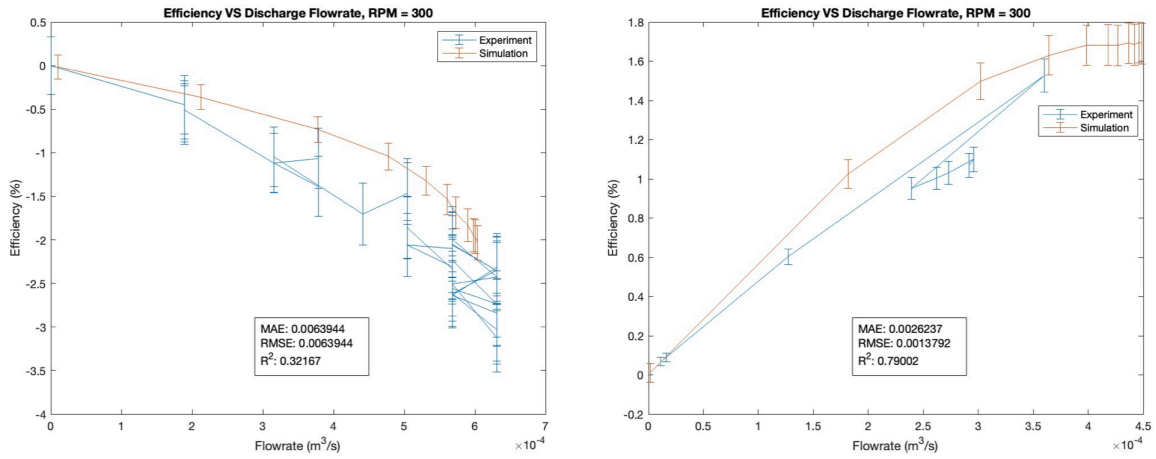

Figure 3.24. Efficiency vs discharge flowrate for the pump with red (left) impeller and gold (right) impeller at 300 RPM

3.1.7 Comparison among All Shaft Speed from 300 to 1800 RPM

Figures 3.25 and 3.26 demonstrate strong overlap between the simulation and experimental data of pump with gold impeller for both the total head and WHP curves. There are still some deviations between the simulation and experimental results for total head and WHP in the case of the pump with the red impeller. These discrepancies are primarily due to errors in the curve fitting, since the parameterized data used in the curve fitting of centrifugal pump (IL) is collected from a part 1 experiment for both pumps. The reason for

that is to avoid overfitting between simulation and experiment results for part 2 experiment, and it also can showcase if the simulation water pump instrument is consistent or not. Clearly, the red pump in this scenario somehow deviates its readings, especially at higher rotational speed.

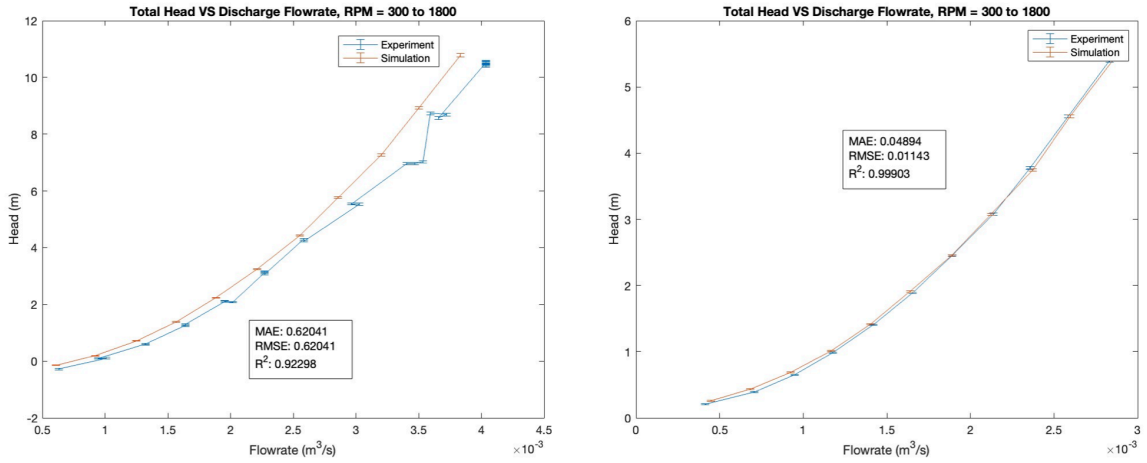

Figure 3.25. Total head vs discharge flowrate for the pump with red (left) impeller and gold (right) impeller from 300 to 1800 RPM

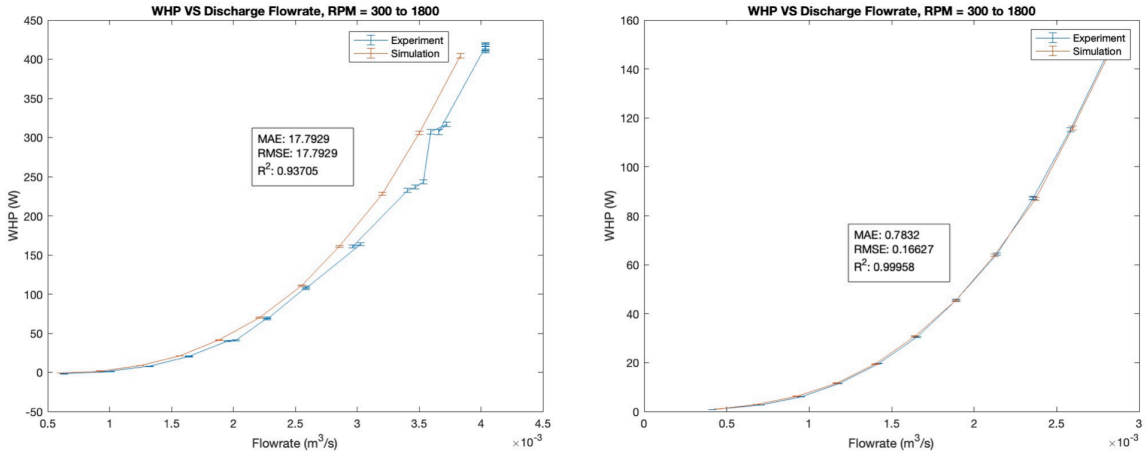

Figure 3.26. WHP vs discharge flowrate for the pump with red (left) impeller and gold (right) impeller from 300 to 1800 RPM

Similarly for figure 3.27 and figure 3.28, the overlapped trend and statistical criteria indicate a strong correlation between the simulation and experiment results. This is primary due to the application of the calibration method to reconcile the differences between the ideal Affinity Law and actual experiment outcomes. In the following section, the Affinity Law will be analyzed again within both simulation setting and actual experiment procedure.

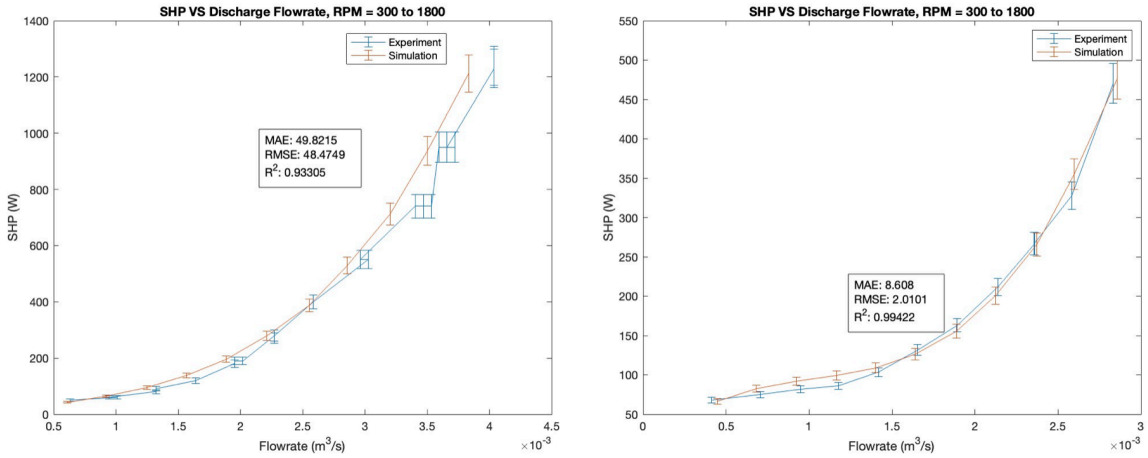

Figure 3.27. SHP vs discharge flowrate for the pump with red (left) impeller and gold (right) impeller from 300 to 1800 RPM

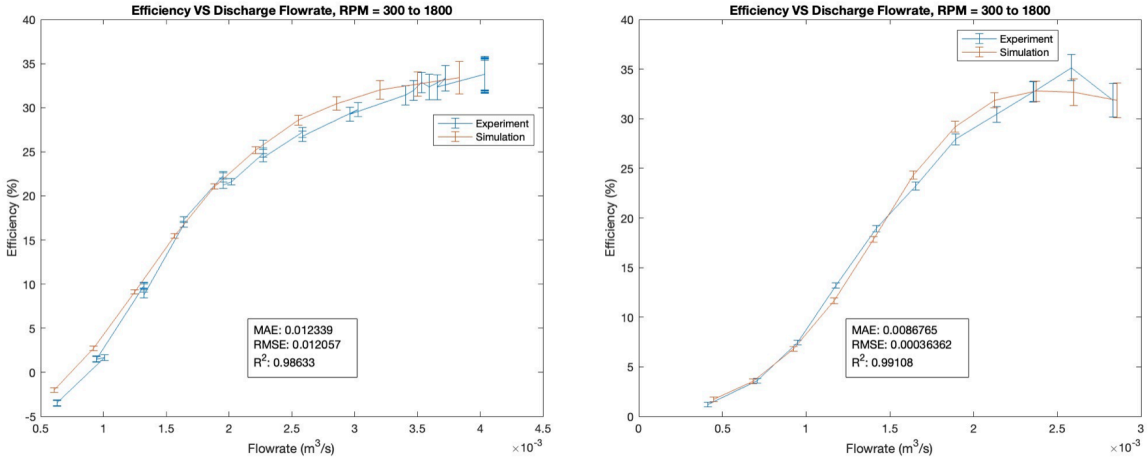

Figure 3.28. Efficiency vs discharge flowrate for the pump with red (left) impeller and gold (right) impeller from 300 to 1800 RPM

3.2 Simulation Results & Analysis for Virtual Experiment Part 1&2:

This section presents the result of the simulation lab activity, derived from conducting part 1 and part 2 of the physical laboratory activities. That means, all procedures, assumptions, and observations are strictly adhered to the outline in the lab manual [17], with the simulated water pump unit serving as the testing subject. As discussed in the preceding chapter, the simulation settings have been designed to accommodate necessary assumptions and meet certain criteria. Additionally, equivalent steps for conducting simulation experiments, analogous to the experimental procedures, have also been outlined.

Measurements are taken using the simulation sensors, which monitor the change in pressure (ΔP) between pump inlet and outlet, water flowrate (Q) throughout the equivalent pipe, as well as the torque (T) applied to the simulated pump. These measurements are recorded 20 times consecutively at shaft speed 1500 RPM without any operation done to the gate valve or shaft speed input. This step is also from experiment part 1 in the lab manual. The purpose of such procedure is to calculate precision uncertainty for each of the parameters, allowing for subsequent computation of total uncertainty of each trial of experiments.

To calculate precision uncertainty, Student's t-test is applied to the set of 20 sample points. Accompanied by the mean and standard deviation of the sample, the precision uncertainty can then be calculated as described in Appendix B. The results are shown in the Table 3.1.

Table 3.1 Calculated precision uncertainties for both pumps (simulation)

Parameter	Gold Pump (1500 RPM)	Red Pump (1500 RPM)
ΔP (Pa)	± 67.82	± 94.45
Q (m^3/s)	± 2.96e-06	± 4.11e-6
Z_1	0	0
Z_2	0	0
T (Nm)	± 0.0024	± 0.0058
ω	0	0

In table 3.1, a direct comparison between precision uncertainties of the simulation pumps with gold and red impeller is presented. These precision uncertainties are also used in the previous section where simulation and experiment results are compared. After observing the table, the precision uncertainties in pressure difference (ΔP), flowrate (Q), and torque (T) are higher than those in the pump with gold impeller. This is likely because the pump with red impeller has a relatively higher power received from drive motor than the other one does, which consequently leads to higher uncertainties of those parameters. For the parameters such as height of the reservoir to the center of the inlet (Z_1), the height of the reservoir to the center of the outlet (Z_2), and the shaft speed (ω), the simulation model assumes their consistency throughout the entire experiment.

With the calculated precision uncertainty, there is only one step away from calculating the total uncertainty which involves figuring out the bias uncertainty. The bias uncertainty has already been provided in the lab manual, and the corresponding specifications for each parameter can be found in Appendix A. For constant parameters, such as heights (Z_1) and (Z_2), as well as shaft speed (ω), bias uncertainties are provided as certain percentages.

Table 3.2 Results with total uncertainties for both pump (simulation)

Parameter	Gold Pump (1500 RPM)	Red Pump (1500 RPM)
Head (m)	4.12 ± 0.02	7.82 ± 0.04
WHP (W)	91.11 ± 0.66	232.32 ± 1.68
SHP (W)	261.16 ± 14.39	678.62 ± 37.25
Efficiency (%)	34.89 ± 1.94	34.23 ± 1.88

In table 3.2, the total uncertainties for the key parameters that depict pump performance have been calculated. Observations reveal that the head experiences the least variation for both pumps, while SHP exhibits the most. This can be attributed to the sensitivity of SHP to changes in torque. Since SHP is a function of the product of torque and shaft speed (assuming constant shaft speed in this case), even only a slight change in the torque can greatly affect SHP.

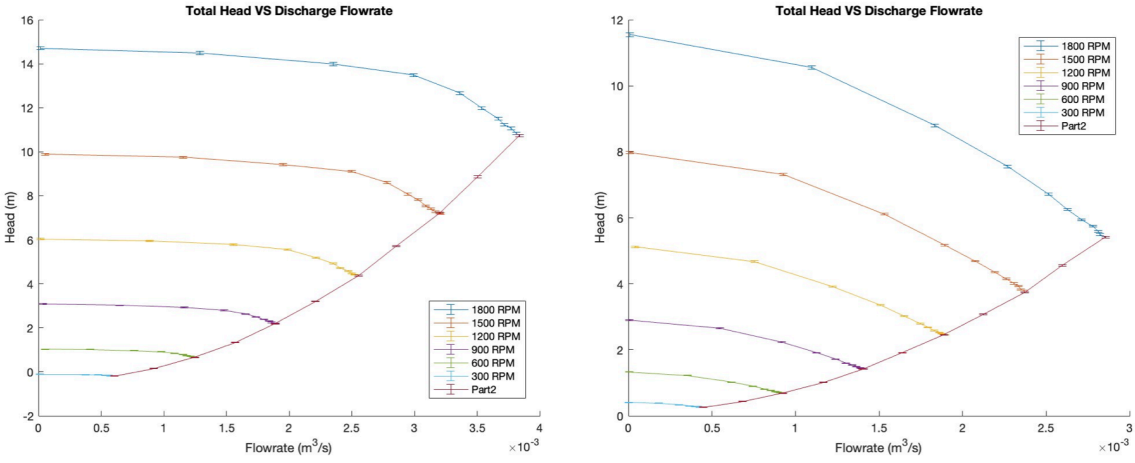

Figure 3.29 Total head vs discharge flowrate for the pump with red (left) impeller and gold (right) impeller

Figure 3.29 illustrates the total head curve for both pumps across seven scenarios, which include shaft speeds of 1800, 1500, 1200, 900, 600, 300 RPM, and an additional scenario

where the shaft speed varies from 300 to 1800 RPM. The first six scenarios derive from simulation experiment part 1, while the varying shaft speed scenario originates from part 2. Observations highlight a perfect alignment of curves from part 1 onto those from part 2, underscoring the consistency across different experimental trials. Furthermore, all curves exhibit relatively small total uncertainties, meaning small variations brought by changes in pressure. It's noteworthy that the pump equipped with the red impeller generates a higher total head across all flowrates and exhibits a broader range of flowrates compared to the pump with the gold impeller.

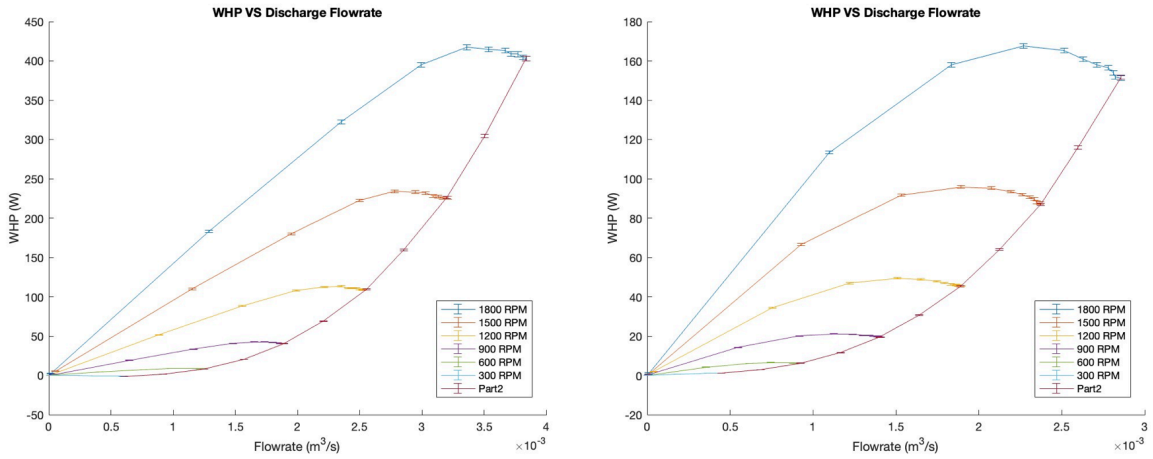

Figure 3.30. WHP vs discharge flowrate for the pump with red (left) impeller and gold (right) impeller

Figure 3.30 depicts the WHP characteristic curvatures over seven trials of experiment. An observable trend within the WHP curves for the pump with the red impeller is that they increase up to a specific flowrate, after which the WHP slightly declines. Although the WHP curves for the pump with the gold impeller follow a similar trend, they exhibit a comparatively lower rate of increase.

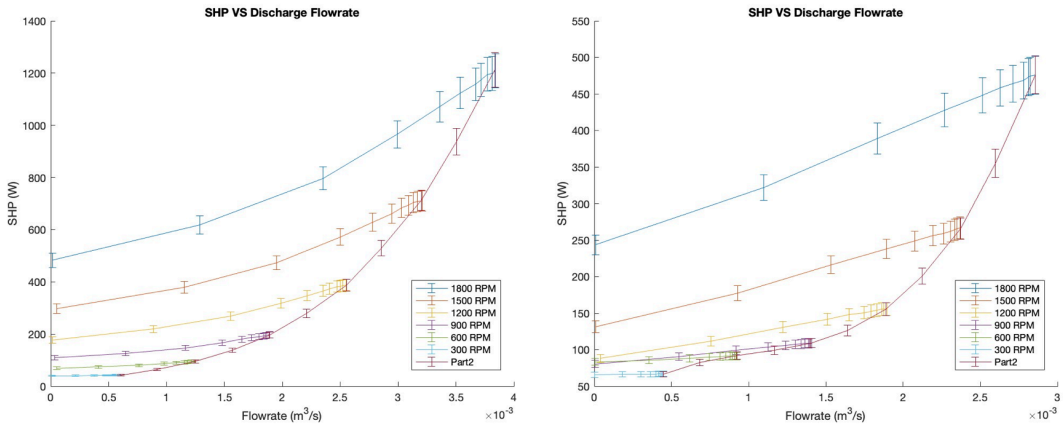

Figure 3.31. SHP vs discharge flowrate for the pump with red (left) impeller and gold (right) impeller

Figure 3.31 illustrates the evolution of SHP for both pumps. The curves display strong similarities to those in the prior WHP figure, but the increase in SHP doesn't cease at a particular flowrate. Instead, both SHP curves continually ascend. This trend is logical, considering that SHP is proportional to both shaft speed and torque. Moreover, as the gate valve or shaft speed inputs are continuously adjusted, larger valve openings in the pipe or increased shaft speeds necessitate more torque, thereby raising the SHP.

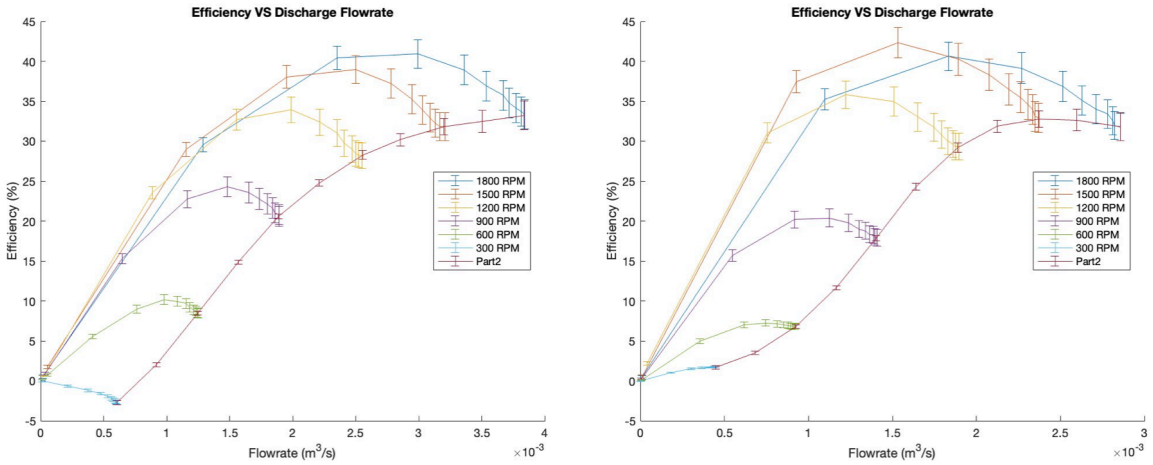

Figure 3.32. Efficiency vs discharge flowrate for the pump with red (left) impeller and gold (right) impeller

Figure 3.32 presents the pump efficiency curves for both devices. From the observation, it seems that both curves align with standard pump performance characteristics. However, the pump with the red impeller strangely demonstrates negative efficiency when operating at a shaft speed of 300 RPM. Additionally, the pump with the gold impeller achieves maximum efficiency at a shaft speed of 1500 RPM instead of the hypothesized 1800 RPM by Affinity Law. The likely cause for the negative efficiency in the red impeller pump could be attributed to the pressure difference data utilized in the calibration between the simulation and experiment, which carries substantial weight. As mentioned in chapter 2, occasional software changes in the original physical unit can influence sensor readings, leading to negative pressure differences. Regarding the maximum efficiency of the pump with the gold impeller, it is likely due to minor errors in the calibration regression curves, most probably the torque calibration.

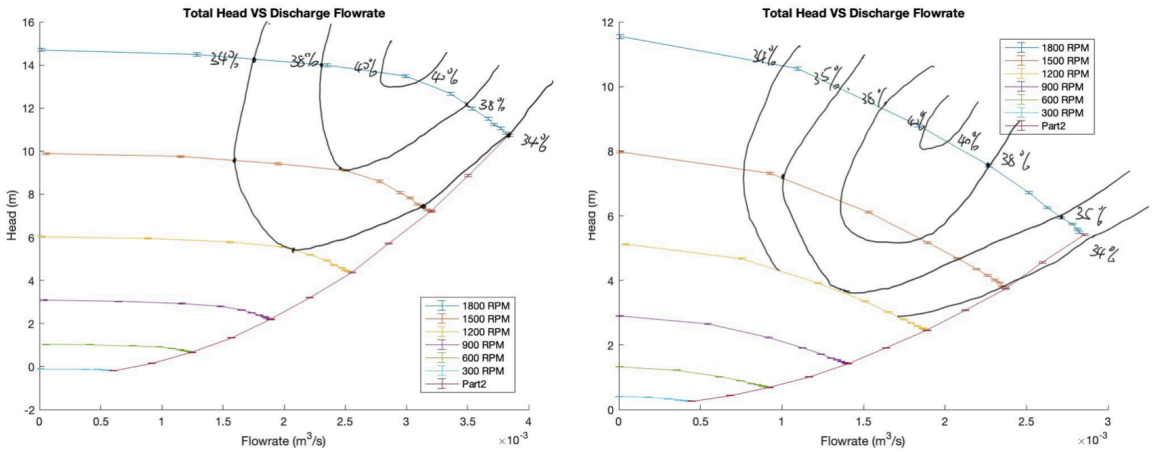

Figure 3.33. Iso-efficiency curve for both pumps

Iso-efficiency curves are displayed in figure 3.33. The curves are roughly hand-drawn according to the trends from both figure 3.29 and figure 3.32. Both curves result in the same maximum efficiency around 40% for simulation result.

Upon completion of the graphical analysis of the simulation results, a comparison is made between simulation data and ideal Affinity Law predictions, including flowrate, total head, and SHP. Since the simulation data is calibrated based the experimental data, the ensuing comparative results should align closely with the differences scrutinized in the original experiment report.

Table 3.3 Similarity analysis for pump with red impeller (simulation)

1500 RPM	Parameter	Prediction	Actual Data	Percent Error (%)
	Flowrate (m^3/s)	0.003207	0.003208	0.0312
	Head (m)	7.48312	7.24727	3.25
	SHP (W)	699.6168	710.3629	1.505
1200 RPM	Parameter	Prediction	Actual Data	Percent Error (%)
	Flowrate (m^3/s)	0.002560	0.002549	0.432
	Head (m)	4.78921	4.43145	8.07
	SHP (W)	358.20384	387.8368	7.64
900 RPM	Parameter	Prediction	Actual Data	Percent Error (%)
	Flowrate (m^3/s)	0.00192	0.001891	1.53
	Head (m)	2.69393	2.2379	20.38
	SHP (W)	151.1172	196.7615	23.20
600 RPM	Parameter	Prediction	Actual Data	Percent Error (%)
	Flowrate (m^3/s)	0.00128	0.00125	2.4
	Head (m)	1.1973	0.7049	69.85
	SHP (W)	44.775	94.6941	52.72
300 RPM	Parameter	Prediction	Actual Data	Percent Error (%)
	Flowrate (m^3/s)	0.00064	0.00060	6.67
	Head (m)	0.2993	-0.1474	303.05
	SHP (W)	5.5969	42.8357	86.93

Table 3.3 outlines the comparison between simulation results and Affinity Law prediction for the pump with the red impeller. It is observed that as shaft speed decreases, the discrepancies between results and prediction increases. As has been repeatedly mentioned, the Affinity Law represents the ideal case, so the discrepancies in total head and SHP are theoretically higher than in flowrate. This is because of the squared and cubic relationships with respect to the ratio in current shaft speed vs referenced shaft speed (1800 RPM).

Table 3.4 Similarity analysis for pump with gold impeller (simulation)

1500 RPM	Parameter	Prediction	Actual Data	Percent Error (%)
	Flowrate (m^3/s)	0.00238	0.00237	0.422
	Head (m)	3.7546	3.7841	0.78
	SHP (W)	275.24	266.75	3.18
1200 RPM	Parameter	Prediction	Actual Data	Percent Error (%)
	Flowrate (m^3/s)	0.001904	0.001894	0.528
	Head (m)	2.4029	2.4557	2.15
	SHP (W)	140.92	155.18	9.19
900 RPM	Parameter	Prediction	Actual Data	Percent Error (%)
	Flowrate (m^3/s)	0.001428	0.001409	1.35
	Head (m)	1.3516	1.4156	4.521
	SHP (W)	59.4516	109.0261	45.47
600 RPM	Parameter	Prediction	Actual Data	Percent Error (%)
	Flowrate (m^3/s)	0.000952	0.000923	3.14
	Head (m)	0.60073	0.6849	12.29
	SHP (W)	17.6153	91.0247	75.66
300 RPM	Parameter	Prediction	Actual Data	Percent Error (%)
	Flowrate (m^3/s)	0.000476	0.000449	6.01
	Head (m)	0.15018	0.2574	41.66
	SHP (W)	2.2019	66.9569	96.71

Similarly, table 3.4 presents the same comparison for the pump with gold impeller. The same findings as in table 3.3 can be spotted in this table as well.

3.3 Analysis from Original Lab Report for Experiment Part 1&2:

This section serves as a complementary analysis to the previous section. The original sample lab report [14], has already thoroughly discussed the comparison between the two physical pumps. Despite this, this section includes additional discussions on datasets that were not covered in the original report, such as those involving shaft speeds of 900, 600, and 300 RPM, as well as any distinct findings comparing to the simulation results. It should be noted that all experimental results calculated in the following section derive from the same experimental steps as in the lab manual, and some of the experimental data are also utilized to parameterize the simulation pumps for the sake of consistency.

Starting with the uncertainty calculation, along with following the exact same procedure as in lab manual, a total of 20 data points at shaft speed of 1500 RPM, including pressure difference (ΔP), flowrate (Q), and torque values (T) are gathered to analyze for their precision uncertainties. The height differences (Z_1) and (Z_2), as well as the shaft speed (ω) are considered negligible in terms of precision uncertainty.

From table 3.5 and table 3.6, the uncertainties are not so much difference than in simulation analysis. This proves that the simulation is capable of conducting uncertainty analysis for the experiment.

Table 3.5 Calculated precision uncertainties for both pumps (experiment)

Parameter	Old Pump (1500RPM)	New Pump (1500RPM)
ΔP (Pa)	± 47.98	± 251.30
Q (m^3/s)	± 1.56e-06	± 2.44e-6
Z_1	Assumed Negligible	Assumed Negligible
Z_2	Assumed Negligible	Assumed Negligible
T (Nm)	± 2.13e-16	± 0.0109
ω	Assumed Negligible	Assumed Negligible

Table 3.6 Results with total uncertainties for both pump (experiment)

Parameter	Old Pump (1500RPM)	New Pump (1500RPM)
Head (m)	3.98 ± 0.02	7.50 ± 0.045
WHP (W)	88.72 ± 0.63	227.11 ± 2.52
SHP (W)	266.53 ± 14.23	690.00 ± 40.31
Efficiency (%)	33.29 ± 1.79	32.91 ± 1.93

From figure 3.34, very similar trends compared to simulation ones can be noticed, with a little bit of disturbance in the pump with red impeller due to the nature of PID control method used in the original physical unit.

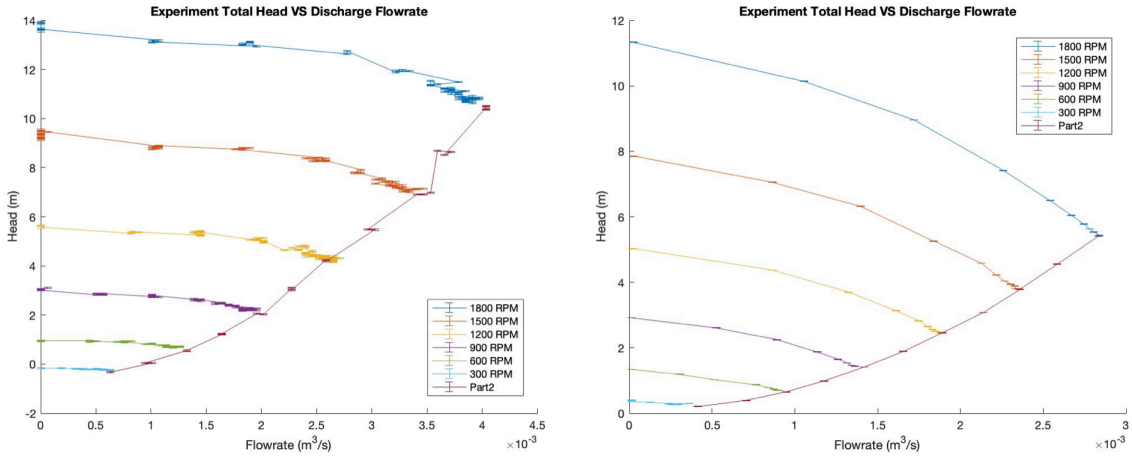

Figure 3.34. Total head vs discharge flowrate for the pump with red (left) impeller and gold (right) impeller

Figures 3.35 and 3.36 offer comparative views of experimental WHP and SHP values for both pumps. A significant observation is the misalignment in the SHP curves for the pump with the gold impeller at 300, 600, and 900 RPM, in relation to the curve from part 2 – an issue that has been mentioned in previous sections. This discrepancy likely stems from the differences in procedures for part 1 and part 2 of the experiment: part 1 involved changing gate valve control while holding the shaft speed constant, while part 2 held the gate valve constant but varied the shaft speed. Since shaft speed is directly controlled by the physical unit's internal built-in software, its impact on the results should be negligible. The inconsistency could therefore be attributed to variations in gate valve control. After each

trial in part 1, the gate valve was fully opened, but the "fully opened" position may not have been consistently achieved in each new trial, leading to the observed discrepancies.

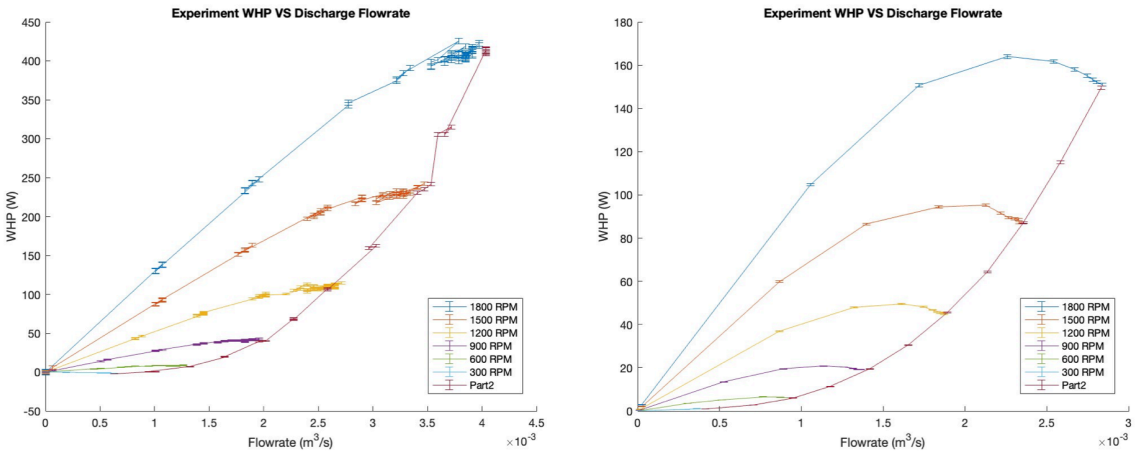

Figure 3.35. WHP vs discharge flowrate for the pump with red (left) impeller and gold (right) impeller

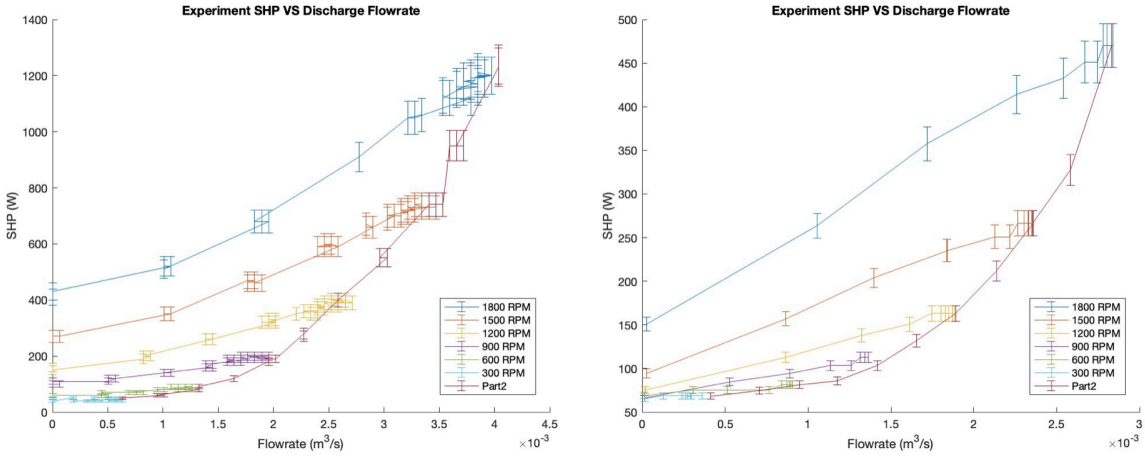

Figure 3.36. SHP vs discharge flowrate for the pump with red (left) impeller and gold (right) impeller

In figure 3.37, despite the variations caused by the mechanism of PID control planted in the pump with red impeller, both efficiency curves provide similar results comparing to the previous showcased in simulation. Using this figure, the iso-efficiency curve can be drawn.

As explained in the simulation section, the resulting efficiency at 300 RPM for the pump with red impeller providing a set of negative values is due to the sensor software updates.

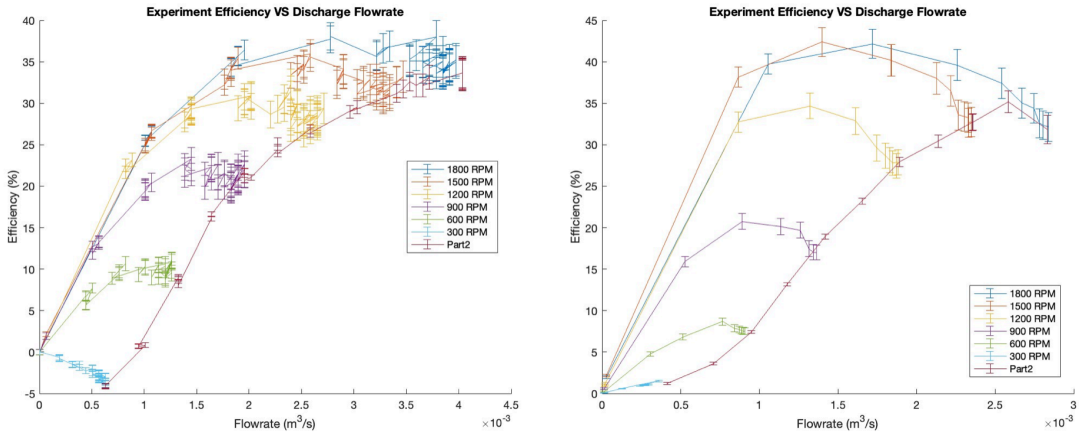

Figure 3.37. Efficiency vs discharge flowrate for the pump with red (left) impeller and gold (right) impeller

The iso-efficiency curves in figure 3.38 resemble closely to the curves in simulation results. The only difference is that the experimental iso-efficiency curve for pump with gold impeller has a slightly larger maximum threshold, which can be the result of calibration error.

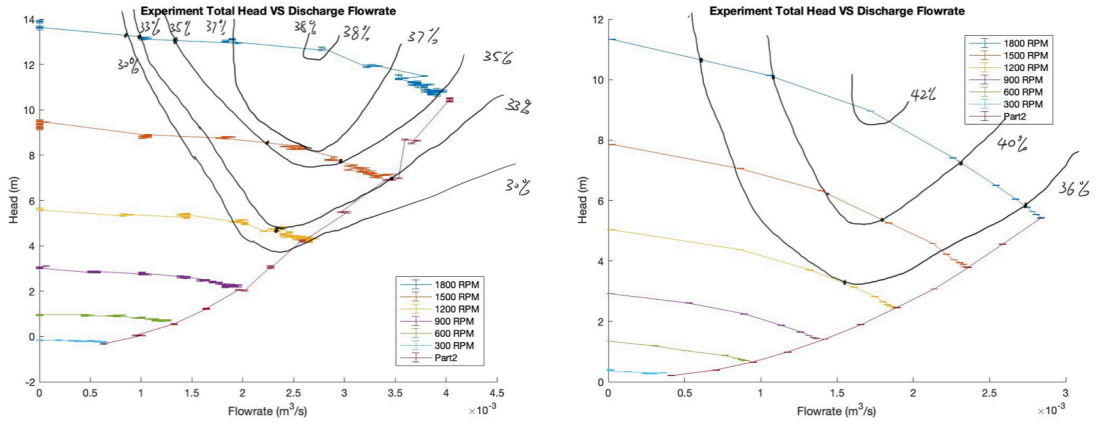

Figure 3.38. Iso-efficiency curve for both pumps

Table 3.7 Similarity analysis for pump with red impeller (experiment)

1500 RPM	Parameter	Prediction	Actual Data	Percent Error (%)
	Flowrate (m^3/s)	0.003207	0.00328	2.23
	Head (m)	7.4783	7.1375	4.77
	SHP (W)	688.66	740.00	6.94
1200 RPM	Parameter	Prediction	Actual Data	Percent Error (%)
	Flowrate (m^3/s)	0.002565	0.002586	8.12
	Head (m)	4.7861	4.2781	11.87
	SHP (W)	352.59	390.00	9.59
900 RPM	Parameter	Prediction	Actual Data	Percent Error (%)
	Flowrate (m^3/s)	0.00192	0.001956	1.84
	Head (m)	2.6922	2.2950	17.3
	SHP (W)	148.75	200.00	25.625
600 RPM	Parameter	Prediction	Actual Data	Percent Error (%)
	Flowrate (m^3/s)	0.00128	0.00120	6.67
	Head (m)	1.1965	0.7371	62.32
	SHP (W)	44.07	90.00	51.03
300 RPM	Parameter	Prediction	Actual Data	Percent Error (%)
	Flowrate (m^3/s)	0.00064	0.00063	1.59
	Head (m)	0.2991	-0.1946	253.70
	SHP (W)	5.51	50.00	88.98

From table 3.7, it can be seen that the percent errors of total head and SHP, like the ones in the simulation results, increase as the shaft speed decrease. In theory, the order of increment (accuracy) between the errors of total head should be close to second order, and the order of accuracy of SHP should be close to third order according to the Affinity Law equations. However, differences in both simulation and experimental do not quite follow that hypothesis. The possible factors could be fluctuations from the data provided by physical units and lack of consideration in simulation towards the realistic scenarios.

Table 3.8 Similarity analysis for pump with gold impeller (experiment)

1500 RPM	Parameter	Prediction	Actual Data	Percent Error (%)
	Flowrate (m^3/s)	0.00236	0.00235	0.426
	Head (m)	3.7748	3.7994	0.647
	SHP (W)	272.11	266.53	2.09
1200 RPM	Parameter	Prediction	Actual Data	Percent Error (%)
	Flowrate (m^3/s)	0.00189	0.00187	1.07
	Head (m)	2.4159	2.443	1.109
	SHP (W)	139.32	163.12	14.59
900 RPM	Parameter	Prediction	Actual Data	Percent Error (%)
	Flowrate (m^3/s)	0.001419	0.001364	4.03
	Head (m)	1.3589	1.4375	5.47
	SHP (W)	58.78	112.84	47.91
600 RPM	Parameter	Prediction	Actual Data	Percent Error (%)
	Flowrate (m^3/s)	0.000946	0.000908	4.18
	Head (m)	0.6040	0.6894	12.39
	SHP (W)	17.42	81.42	78.6
300 RPM	Parameter	Prediction	Actual Data	Percent Error (%)
	Flowrate (m^3/s)	0.000473	0.000411	62.54
	Head (m)	0.15010	0.2059	27.1
	SHP (W)	2.18	68.2089	96.81

From table 3.7 and table 3.8, it can be seen that the percent errors of total head and SHP, like the ones in the simulation results, increase as the shaft speed decrease. In theory, the order of increment (accuracy) between the errors of total head should be close to second order, and the order of accuracy of SHP should be close to third order according to the Affinity Law equations. However, differences in both simulation and experimental do not quite follow that hypothesis. The possible factors could be fluctuations from the data provided by physical units and lack of consideration in simulation towards the realistic scenarios.

3.4 Digital Twin Criteria– Capability and Incapability:

After validating the water pump simulation results against the original laboratory data, it is evident that this simulation model satisfies the digital twin criteria discussed in Chapter 1, which stipulate that the twin should replicate the same functionality of the original and be capable of using device input.

However, the limitations of this simulation lie in its inability to transmit input and output data in real time. The concept of a digital twin extends beyond simply mirroring the physical system for users; it is also expected to predict the lifespan or critical state of the operating unit, thereby providing feedback for maintenance or calibration to achieve a specific outcome. In an ideal scenario, a digital twin would use an internet connection to receive data from the laboratory water pump device. It would visually represent pipe flows using 2D or 3D animations, identify critical values—such as negative total pressure head, backflow, or cavitation effects—and subsequently alert the operation through the interface. Simultaneously, it would transmit corrective data back to the pump, enabling it to adjust sensor output or shut down the entire system for maintenance if necessary. Nonetheless, a significant challenge remains for this ideology: enabling real-time data exchange between the physical pump and the simulation. While the laboratory water pump is equipped with built-in Ethernet access, establishing data communication with external computer devices demands advanced skills. This does not even consider the complexities of remotely controlling the physical pump and ensuring compatibility between MATLAB and the built-in mechatronic software for the sake of data transmission. Thus, this project does not further the implementation of real time data access.

CHAPTER 4

CONCLUSION

Overall, the development of the laboratory water pump simulation has been successfully verified and validated. Boasting features such as 2D schematics, an interactive user interface, and error propagation of sensor readings, this simulation could be integrated into future mechanical engineering experimental courses. This would allow remote students to engage in a 'hands-on' online laboratory experience. Moreover, due to the simulation's rapid operation and nearly transient response time—a stark contrast to the original sensors' PID control—experiments can be conducted within minutes, significantly enhancing efficiency compared to traditional in-person laboratory sessions. Most importantly, this simulation software enables every student to conduct experiments individually, a marked departure from the original group-based format.

However, there are several obstacles that prevent this simulation from perfectly mirroring the physical water pump unit as a digital twin. Firstly, the simulation cannot replicate part 3 of the original experiment, which pertains to the pump cavitation effect, based solely on the experimental data gathered. Although a threshold can be implemented to indicate when cavitation occurs, showing the data only is invaluable for students. The second concern is data transmission, which is integral for establishing a real-time connection, since delivering data remotely from the pump to external computers, and vice versa, is challenging. Lastly, the absence of a system flow animation is regrettable, as it may impact students'

comprehension of the material. Despite these limitations, the simulation does partially satisfy the concept of a digital twin, marking a significant step towards a Virtual Laboratory.

CHAPTER 5

FUTURE WORKS

Several enhancements could be made to this project in the future. The most critical of these is the implementation of the part 3 experiment. Given that this part of the experiment essentially requires students to record data after observing the cavitation effect, it is necessary to develop a way to animate the entire system flow. For example, the elements that need to be animated should include a piping system similar to that in Figure 1.4, water flow within the pipe, an impeller whose speed varies based on flow conditions, and two gate valves controlled by the user. When cavitation occurs, as determined by a threshold calculated from physical experiment data, the water flow will generate bubbles. Although the sign of cavitation happened in simulation will still be threshold-based, this will be supplemented with visual effects. If the aim is to merely improve the existing model, a more detailed analysis, such as machine learning technique, could be conducted to yield more stable results from doing thousands or as many experiments as possible, thereby enhancing the accuracy of simulation inputs.

Owing to time constraints, this project development did not incorporate student feedback. Future analyses should consider this factor, as user opinions are instrumental in steering the project in the right direction. If possible, the feedback process should be first dividing the student population into three groups: those who perform the experiment, those who use the simulation, and those who engage in a hybrid approach (both simulation and experiment). Then, each group will follow the laboratory procedures. Finally, students will

evaluate their experiences based on questions that focus on their understanding of the material and the time efficiency of their corresponding approaches.

REFERENCES

[1] Arizona State University Online. (n.d.). Engineering degrees. Retrieved June 12, 2023, from https://asuonline.asu.edu/study/engineering-degrees/

[2] J.A. Rossiter (2016). Low production cost virtual modelling and control laboratories for chemical engineering students. IFAC-PapersOnLine, 49(6), 230-235. https://doi.org/10.1016/j.ifacol.2016.07.182

[3] J.A. Rossiter (2017). Using interactive tools to create an enthusiasm for control in aerospace and chemical engineers. IFAC-PapersOnLine, 50(1), 9120 https://doi.org/10.1016/j.ifacol.2017.08.1713

[4] Biswas, M. A. R., & Stilwell, B. L., & Reyes, E. (2021, March), Simulated Laboratory-Based Learning In A Thermal Fluid Laboratory Course. Paper presented at ASEE 2021 Gulf-Southwest Annual Conference, Waco, Texas. https://peer.asee.org/36401

[5] Biswas, M. A. R., & Reyes, E. (2021), Thermal Model Development and Control Design Interface of a PEM Fuel Cell for Simulation Based Learning in a Mechanical Engineering Course. Paper presented at ASEE 2021 Gulf-Southwest Annual Conference, Waco, Texas. https://sites.asee.org/se/wp-content/uploads/sites/56/2021/04/2021ASEESE9.pdf

[6] Nikolov, K. A., & M. A. R., & Nguyen, X., & Ortiz V. E. (2021), Simulated Crossflow Heat Exchanger System Using Simulink Modeling. Paper presented at ASEE 2021 Gulf-Southwest Annual Conference, Waco, Texas.

[7] Diaz Herazo, R. E., Obregon Quinones, L. G., & Valencia Ochoa, G. E. (2017). Development of an educational software in MATLAB for transient heat transfer analysis. Contemporary Engineering Sciences, 10(20), 953-961. https://doi.org/10.12988/ces.2017.79102

[8] Okoyeigbo, O., Agboje, E., Omuabor, E., Samson, U. A., & Orimogunje, A. (2020). Design and implementation of a java based virtual laboratory for data communication simulation. International Journal of Electrical and Computer Engineering, 10(6), 5883-5890. https://doi.org/10.11591/ijece.v10i6.pp5883-5890

[9] Dabney, J. B., & Ghorbel, F. H. (2005). Enhancing an advanced engineering mechanics course using MATLAB and Simulink. International Journal of Engineering Education, 21(5), 885-895.

[10] Pradyumna, P. R., Tarun, C. K. S., & Bhanot, S. (2012). Remote experimentation of "No-load tests on a transformer" in electrical engineering. In Proceedings of the 2012 IEEE International Conference on Engineering Education: Innovative Practices and Future Trends (AICERA) (pp. 1-6). https://doi.org/10.1109/AICERA.2012.6306740

[11] Kapilan, N., Vidhya, P., & Gao, X.-Z. (2021). Virtual Laboratory: A Boon to the Mechanical Engineering Education During Covid-19 Pandemic. Higher Education for the Future, 8(1), 31–46. https://doi.org/10.1177/2347631120970757

[12] Fan, Y., Evangelista, A., & Indumathi, V. (2021). Evaluation of remote or virtual laboratories in E-Learning Engineering Courses. In Proceedings of the 2021 IEEE Global Engineering Education Conference (EDUCON) (pp. 136-143). https://doi.org/10.1109/EDUCON46332.2021.9454067

[13] Grieves, M., Vickers, J. (2017). Digital Twin: Mitigating Unpredictable, Undesirable Emergent Behavior in Complex Systems. In: Kahlen, J., Flumerfelt, S., Alves, A. (eds) Transdisciplinary Perspectives on Complex Systems. Springer, Cham. https://doi.org/10.1007/978-3-319-38756-7_4

[14] Mahmmoud S. (2022). Water Pump Lab Report. Unpublished lab report, Arizona State University.

[15] Turbine Technology. (n.d.). FLUIDMechatronix Curriculum [Brochure]. Retrieved from https://www.turbinetechnologies.com/educational-lab-products/pump-lab-with-automation

[16] Pavlou, A., Kurtz, R., & Song, J. (2021). Diagnostic accuracy studies in radiology: How to recognize and address potential sources of bias. Radiology Research and Practice, 2021, 1-10. https://doi.org/10.1155/2021/5801662

[17] Milcarek, R. (2022). Lab Manual – Water Pump. ASU School for Engineering of Matter, Transport, and Energy.

[18] MathWorks. (2020). Pipe (IL) block. MATLAB & Simulink Simscape Documentation. Retrieved from https://www.mathworks.com/help/simscape/ref/pipeil.html;jsessionid=efbaf342a336d1a21465ff7c9b3a

[19] MathWorks. (2020). Orifice (IL) block. MATLAB & Simulink Hydro Power System Toolbox Documentation. Retrieved from https://www.mathworks.com/help/hydro/ref/orificeil.html

[20] MathWorks. (2020). Centrifugal Pump (IL) block. MATLAB & Simulink Hydro Power System Toolbox Documentation. Retrieved from https://www.mathworks.com/help/hydro/ref/centrifugalpumpil.html

[21] Çengel, Y. A., Boles, M. A., Turner, R. H., & Cimbala, J. M. (2019). Thermodynamics: An Engineering Approach. McGraw-Hill Education.

[22] Hibbeler, R. C. (2022). Fluid Mechanics (3rd ed.). Pearson.

[23] Kniffin, K. M., Narayanan, J., Anseel, F., Antonakis, J., Ashford, S. P., Bakker, A. B., Bamberger, P., Bapuji, H., Bhave, D. P., Choi, V. K., Creary, S. J., Demerouti, E., Flynn, F. J., Gelfand, M. J., Greer, L. L., Johns, G., Kesebir, S., Klein, P. G., Lee, S. Y., Ozcelik, H., Petriglieri, J. L., Rothbard, N. P., Rudolph, C. W., Shaw, J. D., Sirola, N., Wanberg, C. R., Whillans, A., Wilmot, M. P., & Vugt, M. V. (2021). COVID-19 and the workplace: Implications, issues, and insights for future research and action. *American Psychologist, 76*(1), 63-77. https://doi.org/10.1037/amp0000716

APPENDIX A

UNCERTAINTY ASSUMPTIONS

Tables provided with the instructions [17], which give uncertainty values and other variables used in calculations throughout the whole experiment.

Performance parameter	Variable	Source of Error	Bias uncertainty
Inlet pressure	P_{in}	Estimated by TA and Lab Manager	0.5% of full scale
Outlet pressure	P_{out}	Estimated by TA and Lab Manager	0.5% of full scale
Height to inlet tube	Z_1	Resolution of tape measure	±0.0625in
Height to outlet tube	Z_2	Resolution of tape measure	±0.0625in
Torque	T	Estimated by TA and Lab Manager	0.5% of full scale
Pump speed	ω	Estimated by TA and Lab Manager	0.25% of full scale
Flowrate	Q	Estimated by TA and Lab Manager	0.5% of full scale

Table 1: Bias uncertainty values for both pump systems and their corresponding source of error

Device name/Variable	Full scale value	Source
Inlet pressure transducer (P_{in})	29.4 Psia	Specified by Manufacturer
Outlet pressure transducer (P_{out})	39.7 Psia	Specified by manufacturer
Flowmeter -old pump	100 gal/min	Estimated by TA and Lab Manager based on experimental data
Flowmeter- new pump	400 L/min	Estimated by TA and Lab Manager based on experimental data
Torque	5 ft-Ibf	Estimated by TA and Lab Manager based on experimental data
Pump Motor	2400 rpm	Estimated by TA and Lab Manager based on experimental data

Table 2: Full scale values of relevant components of the water pump system.

Parameters	Precision uncertainty-old pump (Gold impeller)	Precision uncertainty-new pump (Red impeller)
P_{in}	**To be found by student**	**To be found by student**
P_{out}	**To be found by student**	**To be found by student**
Z1	Student may assume that this precision uncertainty is negligible.	Student may assume that this precision uncertainty is negligible.
Z2	Student may assume that this precision uncertainty is negligible.	Student may assume that this precision uncertainty is negligible.
T	Student may assume that this precision uncertainty is negligible.	Student may assume that this precision uncertainty is negligible.
ω	Student may assume that this precision uncertainty is negligible.	Student may assume that this precision uncertainty is negligible.
Q	**To be found by student**	**To be found by student**

Table 3: Relevant precision uncertainties for both pump systems. Note that you are only required to find the precision uncertainties for the bolded parameters

APPENDIX B

UNCERTAINTY CALCULATION

Uncertainty derivation and calculation procedure based on experimental data as well as the assumption in APPENDIX A.

General Equations for Precision, Bias and Total Uncertainty:

$$\boldsymbol{P} = \sqrt{\left(\frac{\partial y}{\partial x_1}\boldsymbol{P}_{x_1}\right)^2 + \left(\frac{\partial y}{\partial x_2}\boldsymbol{P}_{x_2}\right)^2 + \left(\frac{\partial y}{\partial x_2}\boldsymbol{P}_{x_3}\right)^2 + \ldots + \left(\frac{\partial y}{\partial x_n}\boldsymbol{P}_{x_n}\right)^2}$$

$$\boldsymbol{B} = \sqrt{\left(\frac{\partial y}{\partial x_1}\boldsymbol{B}_{x_1}\right)^2 + \left(\frac{\partial y}{\partial x_2}\boldsymbol{B}_{x_2}\right)^2 + \left(\frac{\partial y}{\partial x_3}\boldsymbol{B}_{x_3}\right)^2 + \ldots + \left(\frac{\partial y}{\partial x_n}\boldsymbol{B}_{x_n}\right)^2}$$

$$\boldsymbol{U} = \sqrt{\boldsymbol{B}^2 + \boldsymbol{P}^2}$$

WHP Precision Uncertainty:

Based on Eq. (2.12) and (2.13), following equations can be derived:

$$\frac{\partial \mathrm{WHP}}{\partial P_1} = -Q$$

$$\frac{\partial \mathrm{WHP}}{\partial P_2} = Q$$

$$\frac{\partial \mathrm{WHP}}{\partial Q} = P_2 + \frac{3\rho Q^2}{2\left(\frac{\pi {D_2}^2}{4}\right)^2} + \rho g Z_2 - P_1 - \frac{3\rho Q^2}{2\left(\frac{\pi {D_1}^2}{4}\right)^2} - \rho g Z_1$$

To Calculate Uncertainty - Final Form: (Note: Values of uncertainty refer to Appendix A)

$$\boldsymbol{P}_{\mathbf{WHP}} = \sqrt{\left(\frac{\partial \mathbf{WHP}}{\partial \boldsymbol{P}_1}\boldsymbol{P}_{in}\right)^2 + \left(\frac{\partial \mathbf{WHP}}{\partial \boldsymbol{P}_2}\boldsymbol{P}_{out}\right)^2 + \left(\frac{\partial \mathbf{WHP}}{\partial \boldsymbol{Q}}\boldsymbol{P}_{\boldsymbol{Q}}\right)^2}$$

WHP Bias Uncertainty:

Based on Eq. (2.12) and (2.13), following equations can be derived:

$$\frac{\partial \mathrm{WHP}}{\partial P_1} = -Q$$

$$\frac{\partial \mathrm{WHP}}{\partial P_2} = Q$$

$$\frac{\partial \mathrm{WHP}}{\partial Q} = P_2 + \frac{3\rho Q^2}{2\left(\frac{\pi {D_2}^2}{4}\right)^2} + \rho g Z_2 - P_1 - \frac{3\rho Q^2}{2\left(\frac{\pi {D_1}^2}{4}\right)^2} - \rho g Z_1$$

$$\frac{\partial \mathrm{WHP}}{\partial Z_1} = -\rho g Q$$

$$\frac{\partial \mathrm{WHP}}{\partial Z_2} = \rho g Q$$

To Calculate Uncertainty - Final Form: (Note: Values of uncertainty refer to Appendix A)

$$\boldsymbol{B}_{\mathbf{WHP}} = \sqrt{\left(\frac{\partial \mathbf{WHP}}{\partial \boldsymbol{P}_1}\boldsymbol{B}_{in}\right)^2 + \left(\frac{\partial \mathbf{WHP}}{\partial \boldsymbol{P}_2}\boldsymbol{B}_{out}\right)^2 + \left(\frac{\partial \mathbf{WHP}}{\partial \boldsymbol{Q}}\boldsymbol{B}_{\boldsymbol{Q}}\right)^2 + \left(\frac{\partial \mathbf{WHP}}{\partial \boldsymbol{Z}_1}\boldsymbol{B}_{Z_1}\right)^2 + \left(\frac{\partial \mathbf{WHP}}{\partial \boldsymbol{Z}_2}\boldsymbol{B}_{Z_2}\right)^2}$$

WHP Total Uncertainty:

$$\boldsymbol{U_{WHP}} = \sqrt{\boldsymbol{B_{WHP}}^2 + \boldsymbol{P_{WHP}}^2}$$

Total Head Precision Uncertainty:

Based on Eq. (2.12), following equations can be derived: (Q can be represented by V·A)

$$\frac{\partial H}{\partial P_1} = -\frac{1}{\rho g}$$
$$\frac{\partial H}{\partial P_2} = \frac{1}{\rho g}$$
$$\frac{\partial H}{\partial Q} = \frac{Q}{(\frac{\pi {D_2}^2}{4})^2 g} - \frac{Q}{(\frac{\pi {D_1}^2}{4})^2 g}$$

To Calculate Uncertainty - Final Form: (Note: Values of uncertainty refer to Appendix A)

$$\boldsymbol{P_H} = \sqrt{\left(\frac{\partial H}{\partial P_1}\boldsymbol{P_{in}}\right)^2 + \left(\frac{\partial H}{\partial P_2}\boldsymbol{P_{out}}\right)^2 + \left(\frac{\partial H}{\partial Q}\boldsymbol{P_Q}\right)^2}$$

Total Head Bias Uncertainty:

Based on Eq. (2.12), following equations can be derived: (Q can be represented by V·A)

$$\frac{\partial H}{\partial P_1} = -\frac{1}{\rho g}$$
$$\frac{\partial H}{\partial P_2} = \frac{1}{\rho g}$$
$$\frac{\partial H}{\partial Q} = \frac{Q}{(\frac{\pi {D_2}^2}{4})^2 g} - \frac{Q}{(\frac{\pi {D_1}^2}{4})^2 g}$$
$$\frac{\partial H}{\partial Z_1} = -1$$
$$\frac{\partial H}{\partial Z_1} = 1$$

To Calculate Uncertainty - Final Form: (Note: Values of uncertainty refer to Appendix A)

$$\boldsymbol{B_H} = \sqrt{\left(\frac{\partial H}{\partial P_1}\boldsymbol{B_{in}}\right)^2 + \left(\frac{\partial H}{\partial P_2}\boldsymbol{B_{out}}\right)^2 + \left(\frac{\partial H}{\partial Q}\boldsymbol{B_Q}\right)^2 + \left(\frac{\partial H}{\partial Z_1}\boldsymbol{B_{Z_1}}\right)^2 + \left(\frac{\partial H}{\partial Z_2}\boldsymbol{B_{Z_2}}\right)^2}$$

Total Head Total Uncertainty:

$$\boldsymbol{U_H} = \sqrt{\boldsymbol{B_H}^2 + \boldsymbol{P_H}^2}$$

SHP Precision Uncertainty is ZERO according to Appendix 4

SHP Bias Uncertainty:

Based on Equation (2.14), following equations can be derived:

$$\frac{\partial \text{SHP}}{\partial \omega} = T$$
$$\frac{\partial \text{SHP}}{\partial T} = \omega$$

To Calculate Uncertainty - Final Form: (Note: Values of uncertainty refer to Appendix A)

$$\boldsymbol{B_{\text{SHP}} = \sqrt{\left(\frac{\partial \text{SHP}}{\partial \omega} B_{\omega}\right)^2 + \left(\frac{\partial \text{SHP}}{\partial T} B_T\right)^2}}$$

SHP Total Uncertainty:

$$\boldsymbol{U_{\text{SHP}} = B_{\text{SHP}}}$$

Pump Efficiency Precision Uncertainty:

Based on Equation (2.15), following equations can be derived:

$$\frac{\partial \eta}{\partial \text{WHP}} = \frac{1}{\text{SHP}}$$

To Calculate Uncertainty - Final Form: (Note: Values of uncertainty refer to Appendix A)

$$\boldsymbol{P_{\eta} = \frac{\partial \eta}{\partial \text{WHP}} P_{\text{WHP}}}$$

Pump Efficiency Bias Uncertainty:

Based on Equation (2.15), following equations can be derived:

$$\frac{\partial \eta}{\partial \text{WHP}} = \frac{1}{\text{SHP}}$$
$$\frac{\partial \eta}{\partial \text{SHP}} = -\frac{WHP}{\text{SHP}^2}$$

To Calculate Uncertainty - Final Form: (Note: Values of uncertainty refer to Appendix A)

$$\boldsymbol{B_{\eta} = \sqrt{\left(\frac{\partial \eta}{\partial \text{WHP}} B_{\text{WHP}}\right)^2 + \left(\frac{\partial \eta}{\partial \text{SHP}} B_{\text{SHP}}\right)^2}}$$

Pump Efficiency Total Uncertainty:

$$\boldsymbol{U_{\eta} = \sqrt{B_{\eta}{}^2 + P_{\eta}{}^2}}$$